NASA Technical Memorandum 87656

Low-Speed Wind-Tunnel Tests of Single- and Counter-Rotation Propellers

Dana Morris Dunham, Garl L. Gentry, Jr.,
and Paul L. Coe, Jr.

APRIL 1986

NASA

NASA Technical Memorandum 87656

Low-Speed Wind-Tunnel Tests of Single- and Counter-Rotation Propellers

Dana Morris Dunham, Garl L. Gentry, Jr.,
and Paul L. Coe, Jr.
Langley Research Center
Hampton, Virginia

National Aeronautics
and Space Administration

**Scientific and Technical
Information Branch**

1986

SUMMARY

A low-speed (Mach 0 to 0.3) wind-tunnel investigation was conducted to determine the basic performance, force and moment characteristics, and flow-field velocities of single- and counter-rotation propellers. The results for advance ratios from 0.7 to 2.3 show that the maximum efficiency for the eight-blade single-rotation propeller occurred when the propeller blade-section angle of attack was between 7.5° and 9.6°. Compared with the eight-blade, single-rotation propeller, a four- by four- (4 × 4) blade counter-rotation propeller with the same blade design produced substantially higher thrust coefficients for the same blade angles and advance ratios. The results further indicated that ingestion of the wake from a supporting pylon for a pusher configuration produced no significant change in the propeller thrust performance for either the single- or counter-rotation propellers.

Comparisons of the normal and side forces produced by the propeller systems inclined at an angle of attack relative to the free-stream flow show that the counter-rotation propeller produced much lower values of side force and substantially higher values of normal force than the single-rotation propeller.

A two-component laser velocimeter (LV) system was used to make detailed measurements of the propeller flow fields. Results show increasing slipstream velocities with increasing blade angle and decreasing advance ratio. Flow-field measurements for the counter-rotation propeller show that the rear propeller turned the flow in the opposite direction from the front propeller and, therefore, could eliminate the swirl component of velocity, as would be expected.

INTRODUCTION

Several aircraft design studies have shown that advanced turboprop-powered aircraft have the potential for significant fuel savings when compared with turbofan-powered aircraft operating under similar conditions (ref. 1). These studies have indicated that both wing- and aft-fuselage-mounted turboprop configurations appear feasible, but that there are many technical uncertainties associated with these designs.

An important design consideration is the selection of either single- or counter-rotation propellers. Counter-rotation propellers are of interest for both pusher and tractor configurations because of their potential for higher efficiency due to recovery of the energy lost to slipstream swirl. Propeller configuration selection will depend on trade-offs between acoustics, weights, and aerodynamics of the engine installation.

Although there have been decades of experience with propeller-driven aircraft, this experience has been obtained for configurations that operated at lower cruise speeds and used propellers having significantly lower power loadings than those presently being considered. Aside from the questions of propeller performance and efficiency, there is considerable uncertainty regarding the impact of a high-disk-loading turboprop installation on aircraft stability and control during the takeoff, climb, and approach phases of flight.

This investigation was conducted to provide baseline information regarding the performance, force and moment characteristics, and flow fields of isolated single- and counter-rotation turboprop/nacelles over an angle-of-attack range from 0° to 20° for a range of advance ratios from 0.7 to 2.3. The tests were conducted in the Langley 4- by 7-Meter Tunnel for a range of Reynolds numbers (based on propeller blade chord) from 0.15×10^6 to 0.48×10^6.

SYMBOLS

All data have been reduced to coefficient form and are presented in the body axis system shown in figure 1. Symbols used for computerized data listings are given in parentheses.

C_N	(CNF)	normal-force coefficient, $F_N/q_\infty S$
	(CPM)	pitching-moment coefficient, $M_Y/q_\infty Sd$
C_n	(CYM)	yawing-moment coefficient, $M_Z/q_\infty Sd$
C_P	(CP)	power coefficient, $P/\rho n^3 d^5 = 2\pi C_Q$
C_Q		torque coefficient, $Q/\rho n^2 d^5$
	(CRM)	rolling-moment coefficient
C_T	(CT)	thrust coefficient, $T/\rho n^2 d^4$
C_Y	(CSF)	side-force coefficient, $F_Y/q_\infty S$
d		propeller diameter, ft
F_N		normal force, lbf
F_Y		side force, lbf
J	(J)	propeller advance ratio, V_∞/nd
M_Y		pitching moment, ft-lbf
M_Z		yawing moment, ft-lbf
n		propeller rotational speed, rps
P		power, hp
Q		torque, ft-lbf
q_∞		free-stream dynamic pressure, psf
R		propeller radius, d/2, ft
r		radial distance measured from axis of rotation
S		propeller disk area, ft^2

T		thrust force, lbf
u		axial velocity, fps
V_∞		free-stream velocity, fps
v		radial velocity, fps
w		tangential velocity, fps
x		axial distance
$\alpha_{b.75}$		blade-section local angle of attack at station 0.75R
α_n	(ALPHA)	angle of attack of nacelle, deg
$\beta_{.75}$		geometric blade angle defined at station 0.75R, deg
β_n		angle of sideslip of nacelle, deg
η		propeller efficiency, JC_T/C_P
ρ		free-stream density, slugs/ft^3
ϕ		swirl angle, $\tan^{-1}(w/u)$, deg
$\phi_{.75}$		geometric swirl angle defined at station 0.75R (see fig. 21)

Abbreviations:

CR	counter rotation
CRP,P	counter-rotation pusher, pylon mounted
CRT,S	counter-rotation tractor, sting mounted
LV	laser velocimeter
SR	single rotation
SRP,P	single-rotation pusher, pylon mounted
SRT,S	single-rotation tractor, sting mounted

MODEL

The dimensional characteristics of the nacelle used with the single- and counter-rotation propellers are listed in table I and shown in figure 2. All propeller blades tested were an SR-2 design jointly developed by Hamilton Standard and the NASA Lewis Research Center. The planform and twist distribution for the SR-2 propeller blades are available in reference 2. The hubs for both the single-rotation (SR) and counter-rotation (CR) systems permitted operation with two-, four-, or eight-blade propellers over a range of blade reference angles from -2° to 60°. The

blade reference angle $\beta_{.75}$ is the angle between the plane of rotation and the blade zero-lift line measured at the 0.75 blade radius. The single-rotation propeller was 1.408 ft in diameter and the counter-rotation propeller was 1.342 ft in diameter.

The propellers were powered by a 29-hp (at 10 000 rpm) water-cooled electric motor housed in a nacelle having a maximum outside diameter of 6 in. There were two different front ends for the nacelle (table I): the first for use with the single-rotation propeller and the second for use with the counter-rotation propeller and its gearbox. The single-rotation propeller rotated clockwise looking upstream. The gearbox for the counter-rotation system contained a spider gear system consisting of two gears and two pinions to drive the rear propeller in the opposite direction from the front propeller and at the same rotational speed. The front propeller was driven clockwise looking upstream, and the rear propeller was driven counterclockwise. The spacing between the front and rear propellers was 2.31 in.

There were two different mounting arrangements for the nacelle: a sting mount (with a fairing from the nacelle to the sting) and a pylon mount (in which the nacelle was attached to an airfoil-shaped pylon that attached to the sting via an adapter), as shown in figure 3. The pylon mount permitted the propeller to be tested in the pusher configuration. The pylon had a tapered planform with an NACA 0012 airfoil section. The chord length of the pylon at the nacelle was 12.5 in. Ordinates for the nacelle sting adapter and the nacelle aft fairing, which was used with the pylon-mounted configurations, are provided in table I. A six-component strain-gauge balance was mounted at the locations shown in figure 2 and was used to measure aerodynamic forces and moments.

FACILITY

The tests were conducted in the Langley 4- by 7-Meter Tunnel, which has a closed test section measuring 14.50 ft high, 21.75 ft wide, and 50 ft long. This is a closed-circuit atmospheric wind tunnel allowing open or closed test-section operation, and it is described in detail in reference 3. Tests using the 12-W argon-ion laser velocimeter (LV) described in reference 3 were conducted in the open test-section configuration with the LV system located outside the tunnel-flow shear layer, as shown in the test-section plan view in figure 4. The entire optics package for the LV, which operates in 180° backscatter mode, is mounted on the x-y traversing platform shown in figure 5. The LV data acquisition system can simultaneously acquire two channels of LV data and one channel of auxiliary data. Because the propeller/nacelle system was axisymmetric, the two-component LV system could be used to measure three velocity components. The axial and radial components of velocity were obtained by making measurements in a vertical plane passing through the propeller/nacelle axis, and the axial and tangential components of velocity were obtained by making measurements in a horizontal plane.

Velocity measurements were sampled at each location for a period of 1 min. These data were then statistically processed for mean velocity, standard deviation, and skew. The data presented herein are for the mean velocity.

TESTS

Tests for the eight-blade single-rotation propeller/nacelle system were conducted for blade reference angles $\beta_{.75}$ of 30.45°, 40.30°, and 50.15°; for comparative purposes, a four-blade single-rotation propeller was also tested at

$\beta_{.75}$ = 40.30°. (For brevity, these two propellers are occasionally referred to as "8-blade" and "4-blade," respectively, in the figures.) The counter-rotation propeller was tested with four blades per hub (designated "4 × 4," which gave a total of eight blades) for a blade reference angle of 41.34°. For comparative purposes, the counter-rotation propeller was also tested as an 8 × 8 blade system (having a total of 16 blades) with $\beta_{.75}$ = 41.34°. Both the single- and counter-rotation propellers were tested at nacelle angles of attack of 0°, 10°, and 20°. The propeller advance ratio was varied from 0.7 to 2.3 by changing both propeller rotational speed and wind-tunnel velocity. The variation in wind-tunnel velocity (63 to 101 fps) resulted in dynamic pressures ranging from 4.5 to 12 psf. The combination of propeller rotational speed and tunnel free-stream velocity resulted in a range of Reynolds numbers (based on blade chord) from 0.15×10^6 to 0.48×10^6. An appendix is presented as a data supplement and includes a listing of the various test conditions (table AI) and a tabular listing of data (table AII).

The electric motor used in these tests resulted in maximum propeller power loadings (P/d^2) of 14.6 and 16.1 hp/ft^2 for the single-rotation and counter-rotation propellers, respectively. These power loadings are substantially lower than the full-scale values currently being considered for advanced turboprop applications. However, reference 4 shows that it is possible to match correctly the propeller characteristics in coefficient form, and thereby to simulate the thrust and power coefficients and flow-field characteristics for the highly loaded advanced turboprop concepts if the effects of Reynolds number and Mach number are neglected. Under this assumption, a valid wind-tunnel simulation of the performance of a full-scale propeller may be obtained by matching the nondimensional power loading ($P/d^2q_\infty V_\infty$) of the model to the full-scale values.

RESULTS AND DISCUSSION

Effect of Blade Angle on Propeller Performance

Figure 6 presents the basic performance characteristics of the eight-blade single-rotation propeller as a function of advance ratio for blade angles of 30.45°, 40.30°, and 50.15°. The data show an increase in thrust and in power required as blade angle increases. The leveling off of both thrust and power coefficient curves for the higher blade angles at low advance ratios indicates that a portion of the propeller blade may be stalled, although studies were not conducted to verify this possibility.

According to classical propeller theory, as blade angle increases, the maximum efficiency occurs at higher advance ratios. This allows propellers with variable pitch to be operated at the optimum blade angle (and therefore blade-section angle of attack) to produce maximum efficiency at a given advance ratio. The efficiency of the propeller is based on an integration of the aerodynamic performance of each local blade section and is influenced by the distribution of section angle of attack along the blade. Figure 7 illustrates the relationship of blade-section angle of attack, blade angle, and advance ratio J. If the induced inflow velocity is neglected, the velocity seen by the propeller at the 0.75 radial station is a vector sum of the rotational speed at that section ($0.75\pi nd$) and the free-stream velocity (V_∞), and the result is a blade-section angle of attack that can be written as

$$\alpha_{b.75} = \beta_{.75} - \tan^{-1}\left(\frac{J}{0.75\pi}\right)$$

Using this relationship and the data from figure 6 for $\beta_{.75} = 30.45°$ and $40.30°$, the maximum measured propeller efficiency occurred for $\alpha_{b.75} = 7.5°$ and $9.6°$, respectively.

Comparison With Other Experimental Data

Figure 8 shows the variation of thrust coefficient and power coefficient with advance ratio as measured during the present tests compared with performance data provided by the NASA Lewis Research Center for a 2-ft-diameter eight-blade SR-2 propeller. Reference 2 describes the tests performed at the Lewis Research Center but does not include the data provided herein. In addition, figure 8 also presents data from reference 4 for conditions that duplicated the present test conditions and blade angle. As shown, good agreement exists between the three data sets.

Propeller Flow-Field Results

Propeller data such as thrust and power coefficients and efficiency are normally presented as a function of propeller advance ratio. The effect of advance ratio on the slipstream velocities produced by the eight-blade single-rotation propeller is presented in figure 9, which is a comparison of the nondimensional axial and tangential velocity components and swirl angle for two advance ratios. The measurement plane was located 0.148R (1.25 in.) behind the propeller plane.

The data show that the slipstream axial and tangential velocities were higher at the lower advance ratio (higher thrust), as expected. Resolved into vector form, these increases result in a significantly greater swirl angle (the angle between the resolved vector and the axial direction) for the lower advance ratio (higher thrust) condition, as shown in figure 9. The maximum swirl angles measured were 18.4° for $J = 0.86$ and 10.2° for $J = 1.18$. Also note that the axial velocity is less than the free-stream value at the propeller tip and that the tangential velocity is positive outboard of the tip. This pattern appeared consistently throughout the single-rotation data. The fact that the axial velocity is less than the free-stream velocity may be the result of the tip vortex, as suggested in references 5 and 6 where the data exhibited similar trends.

Nondimensional velocities for $\beta_{.75} = 40.30°$ at an advance ratio of 1.18 are shown for three longitudinal measurement stations in figure 10, and the nondimensional velocities for an advance ratio of 0.86 are shown in figure 11. In both cases, the axial and tangential velocities show the expected increase with increasing distance downstream of the propeller as the slipstream accelerated. Radial velocity measurements were made for $J = 1.18$ and are shown in figure 10. The flow toward the nacelle is shown by negative values of v/V_∞ and indicates slipstream contraction. The large positive radial velocity behind the blades near the spinner is caused by the flow over the nacelle curvature.

Effect of Blade Angle on Propeller Flow Field

A comparison of the nondimensional axial and radial velocity components for $\beta_{.75} = 30.45°$ and $40.3°$ is shown in figure 12. The measurement plane was located 0.148R (1.25 in.) behind the propeller plane. The data show a higher axial velocity

(and consequently thrust coefficient) for the higher blade angle. The negative radial velocity near the propeller tip indicates the stronger slipstream contraction for the higher blade angle case.

Comparison of Single- and Counter-Rotation Tractor Propellers

The objective of the counter-rotation propeller system was to obtain increased efficiency by recovering the energy lost due to slipstream swirl with the single-rotation propeller. At the time that the present investigation was conducted, a suitable strain-gauge balance was not available for measuring the torque of the front and rear counter-rotating blade sets, although accurate thrust measurements could be made. As a result, power coefficients for the counter-rotation turboprop system could not be calculated and only a limited number of conditions were investigated. Figure 13 shows the variation of thrust coefficient with advance ratio for the single- and counter-rotation tractor propellers at a blade angle of approximately 40°. At the same advance ratio, the 4 × 4 (eight blades total) counter-rotation propeller produced a substantially higher thrust coefficient than the eight-blade single-rotation propeller. However, the power coefficient was not measured for the counter-rotation propeller, so no conclusion can be reached on the comparative efficiencies.

The nondimensional velocities for the 4 × 4 blade counter-rotation tractor configuration are shown in figure 14. The blades for both of the propellers were set at $\beta_{.75} = 41.34°$ and the advance ratio was 1.21. The axial velocity measurements show the expected acceleration through the two blade rows and farther downstream. As was the case for the single-rotation propeller, axial flow at the tip is less than the free-stream value. Also, the axial velocity data show a strong slipstream contraction within a distance of 1 diameter behind the propellers. This strong slipstream contraction is also seen in the large negative values of radial velocity just aft of the propeller. At the far downstream station, the radial velocity has only a small region of negative flow at the edge of the slipstream. The tangential velocity is positive behind the front propeller and negative behind the rear propeller, indicating that for these propeller blade settings the second propeller overcompensated for the swirl induced into the slipstream by the front propeller.

A direct comparison of the nondimensional axial, radial, and tangential velocity components and the swirl angle for the single- and counter-rotation systems is shown in figure 15. This comparison is presented for the counter-rotation tractor configuration with $\beta_{.75} = 41.34°$ and for the single-rotation tractor data of figure 9. The data show comparable axial velocities; however, the counter-rotation thrust coefficient was appreciably higher. As shown, for these counter-rotation blade settings the net swirl for the counter-rotation propeller was in the opposite direction from that for the single-rotation propeller. Data for the counter-rotation propellers were obtained at more radial stations than for the single-rotation propeller, and the counter-rotation data show details of the flow not evident in the single-rotation measurements. For example, both the radial and tangential components show a spike between 0.8 and 1.0 radius that is only slightly evident in the single-rotation data. This probably indicates the location of the propeller tip vortex, and data for additional measurement locations between 0.8R and 1.0R for the single-rotation condition would be expected to show similar characteristics.

Comparison of Tractor and Pusher Propellers

Figures 16 and 17 present a comparison of the tractor and pusher modes of operation for the single- and counter-rotation propellers. For the conditions investigated, the data show that the thrust performance of the pusher and tractor propellers was approximately equal within the accuracy of the data. For the pusher configuration, the propeller/nacelle was supported by the pylon arrangement shown in figure 3. Note that for the conditions tested, the pylon was also subject to angle-of-attack effects. Based on the data of figures 16 and 17, it appears that ingestion of the pylon wake for a nacelle angle of attack of 10° had no measurable effect on thrust performance for advance ratios below 1.7. Because individual blade loads were not measured during the present series of tests, the impact of the pylon wake on cyclic blade loading is unknown.

No LV measurements were made for the pylon-mounted counter-rotation pusher configuration during the present investigation. However, the same propeller/nacelle/pylon model was mounted on a turboprop transport in a pusher configuration for the tests reported in reference 4. For this case, the flow into the propeller should be influenced by the wing as well as by the nacelle and pylon. The LV measurements were made at two axial stations, 0.442R (3.56 in.) and 2.00R (16.1 in.) aft of the front propeller plane of rotation. A schematic of the mounting arrangement is shown in figure 18.

The nondimensional velocities for the aircraft-mounted counter-rotation pusher configuration for $\beta_{.75} = 41.34°$ at an advance ratio 1.21 are shown in figure 19. The LV survey was made across the entire propeller slipstream at the 2.00R axial station. Centerline data (r/R = 0) for this axial station 1 propeller diameter downstream indicate that the axial velocity behind the nacelle and spinner had reached the free-stream value. The measurements denoted by an "x" in the symbol square were taken on the opposite side of the nacelle centerline from the data denoted by the open symbol. The negative tangential velocities across the entire propeller wake indicate that the wake flow is no longer axisymmetric and the swirl has been dominated by the wing downwash.

The effect of the wing downwash can be seen in figure 20, in which the nondimensional velocities behind the rear propeller are plotted for both the tractor and pusher configurations. These measurements were made above the nacelle. The downwash from the wing flow field produced a vertical displacement of the propeller slipstream for the counter-rotation pusher configuration relative to the tractor configuration. No tangential velocity data at this axial station are available for the pusher configuration.

Propeller/Nacelle Normal Force, Side Force, and Yawing Moment

The propeller normal force that occurs at angle of attack is produced by the turning of the flow through the propeller disk, whereas the yawing moment and side force are due primarily to a nacelle crossflow. The origin of these various loads can be understood by referring to figure 21. Consider a propeller disk at nacelle angle of attack α_n as shown in the figure. At positive nacelle angles of attack, the downgoing blade sections experience an increased section angle of attack and the upgoing blade sections experience a reduced angle of attack. The blades on the downgoing side of the propeller disk therefore produce greater thrust than those on the upgoing side. The pressure behind the propeller disk on the downgoing side is consequently increased relative to the upgoing side. This pressure differential produces

a side force on the nacelle and creates a crossflow on the nacelle that contributes to the yawing moment and side force.

In order to substantiate the existence of this crossflow, the single-rotation propeller/nacelle model was yawed 8° toward the LV system, and the flow velocities were measured above and below the nacelle centerline 2.0R (16.9 in.) downstream of the propeller plane. Since the propeller/nacelle is axisymmetric, this was equivalent to looking down on the system at angle of attack. The LV velocity measurements are shown in vector form in figure 22 where the root of the vector denotes the measurement location, the length shows the magnitude, and the orientation indicates the flow direction. These measurements show that the flow direction in the slipstream at this downstream location was toward the nacelle at an angle of 3° behind the downgoing blade, and it was away from the nacelle behind the upgoing blade. The measured propeller/nacelle side-force increment was comparable to the measured normal force on the nacelle alone (blades off) at an angle of attack of 3°. This use of the LV system as a diagnostic tool in conjunction with other measurements is an illustration of the value of such a system for research facilities.

Figure 23 presents the variation of the normal-force, yawing-moment, and side-force coefficients with respect to thrust coefficient for the eight-blade single-rotation propeller and for the 4 × 4 counter-rotation propeller at approximately the same conditions. The counter-rotation propeller system had lower side force than the single-rotation propeller; however, the counter-rotation propeller system produced a substantially higher normal-force coefficient. From this we conclude that the counter-rotation propeller system was more effective than the single-rotation system in turning the flow through the propeller disks; this may be due in part to the higher efficiency of the counter-rotation system achieved by recovery of the swirl losses. Although some crossflow velocity remained in the counter-rotation propeller slipstream as indicated by the side-force coefficient, it would be expected that the pusher configuration (with the nacelle forward of the propeller) would totally eliminate the yawing moment and side force.

SUMMARY OF RESULTS

The results of low-speed wind-tunnel tests to determine the basic performance, force and moment characteristics, and flow-field characteristics of an eight-blade single-rotation propeller and a four- by four- (4 × 4) blade counter-rotation propeller with SR-2 blades may be summarized as follows:

1. Laser velocimeter (LV) measurements documented the eight-blade single-rotation propeller flow-field velocities for changes in blade angle and advance ratio and documented the velocities of one operating condition of the 4 × 4 blade counter-rotation propeller flow field for comparison.

2. At a nominal blade angle of 40°, the 4 × 4 counter-rotation propeller produced substantially higher thrust coefficients than the eight-blade single-rotation system. The LV measurements made between the two blade rows, and aft of the second blade row, showed that the counter-rotation propeller system was effective in changing flow swirl direction.

3. Ingestion of the pylon wake for the pusher configurations of both the single- and counter-rotation propellers had no serious detrimental effect on the propeller thrust performance.

4. Comparisons of the normal and side forces produced by the propeller systems at angle of attack show that the counter-rotation propeller produced substantially higher values of normal force than the single-rotation propeller. Conversely, the single-rotation propeller/nacelle produced substantially higher values of side force than the counter-rotation propeller/nacelle.

5. The side force produced for the single-rotation propeller was found to be due to the crossflow on the nacelle. This crossflow is a result of the propeller disk operating at angle of attack.

NASA Langley Research Center
Hampton, VA 23665-5225
March 7, 1986

APPENDIX

DATA SUPPLEMENT

As an aid to the reader, this data supplement provides the wind-tunnel test conditions and tabulated aerodynamic data.

TABLE AI.- TEST CONDITIONS

Run	Configuration	Number of blades	$\beta_{.75}$, deg	α_n, deg	β_n, deg
71	SRT,S	4	40.30	0	0
72	↓	8	↓	0	0
73	↓	↓	↓	10	0
74	↓	↓	↓	0	10
75	↓	↓	50.15	0	0
77	↓	↓	30.45	0	↓
92	CRT,S	4 × 4	41.34/41.34	10	↓
93	↓	4 × 4	↓	20	↓
106	↓	8 × 8	↓	0	↓
112	↓	4 × 4	↓	0	↓
119	CRP,P	4 × 4	↓	0	↓
120	↓	4 × 4	↓	10	↓
127	↓	4 × None	41.34	0	↓
128	↓	8 × None	41.34	0	↓
129	↓	8 × 8	41.34/41.34	0	↓

TABLE AII.- TABULATED AERODYNAMIC DATA

RUN= 71

ALPHA	J	CP	CT	CPM	CNF	CYM	CSF	CRM
.01	1.7594	-.0005	-.0897	-.0684	-.0488	-.0062	-.0147	.0001
.01	1.6168	.1141	-.0112	-.0617	-.0460	-.0011	-.0013	-.0177
-.06	1.4969	.2265	.0399	-.0457	-.0828	-.0076	-.0200	-.0410
-.02	1.4228	.2750	.0834	-.0629	-.0780	.0161	.0240	-.0550
-.02	1.3453	.3228	.1236	-.0659	-.0761	.0233	.0190	-.0723
.05	1.2318	.4099	.1772	-.0718	-.0950	.0118	.0172	-.1095
.01	1.1687	.4683	.2126	-.0758	-.0832	.0342	.0396	-.1390
-.06	1.0832	.5312	.2493	-.1150	-.0701	-.0032	.0262	-.1835
.39	.9809	.5881	.3095	-.0696	-.0300	.0883	.0699	-.2477
.09	.8743	.6270	.3282	-.0741	-.0619	.0888	.0954	-.3324
.05	.7965	.6765	.3472	-.1020	-.0733	.1218	.1528	-.4321
.01	.7078	.7154	.3714	-.1503	-.0800	.1249	.1887	-.5788

RUN= 72

ALPHA	J	CP	CT	CPM	CNF	CYM	CSF	CRM
.05	2.1548	-.4102	-.2817	-.0935	-.0678	-.0447	-.0383	.0358
-.06	1.7213	.1094	.0009	-.0911	-.0661	.0011	-.0193	-.0150
-.06	1.5799	.2130	.0904	-.0938	-.0296	-.0227	-.0286	-.0346
-.06	1.4850	.3654	.1595	-.1079	-.0485	-.0189	-.0062	-.0671
.16	1.4080	.4595	.2402	-.0801	-.0544	.0065	-.0002	-.0939
-.06	1.3352	.5573	.2753	-.1115	-.0632	.0073	-.0051	-.1267
-.02	1.2474	.6247	.3205	-.1022	-.0359	.0324	.0267	-.1627
.01	1.1783	.7144	.3771	-.1072	-.0684	.0166	.0154	-.2085
.09	1.0814	.8215	.4317	-.1226	-.0730	.0808	.0574	-.2847
.05	.9637	.8893	.4719	-.1009	-.0444	.0546	.0714	-.3880
.09	.8832	.9653	.5114	-.1502	-.0645	.0796	.1124	-.5015
.05	.7913	.9907	.5246	-.1794	-.1188	.0508	.1152	-.6412
.20	.6986	1.0193	.5441	-.1397	-.1112	.1297	.1684	-.8463

TABLE AII.- Continued

RUN= 73

ALPHA	J	CP	CT	CPM	CNF	CYM	CSF	CRM
10.18	2.1074	-.4738	-.3374	.2525	.0659	.1198	.0827	.0432
9.98	1.7778	.0639	-.0581	.2576	.0843	.0519	.0217	-.0082
10.10	1.6071	.2658	.0819	.2799	.0617	.0310	.0001	-.0417
10.14	1.5002	.3719	.1635	.2759	.0714	-.0143	-.0193	-.0670
10.14	1.4289	.4805	.2028	.2750	.0982	-.0255	-.0408	-.0954
10.02	1.3354	.5369	.2498	.2979	.0719	-.0817	-.0550	-.1225
10.18	1.2425	.6262	.3225	.3077	.0861	-.0782	-.0609	-.1644
10.18	1.1571	.7270	.3648	.3420	.0953	-.0753	-.0847	-.2201
10.18	1.0457	.7452	.3889	.3735	.1295	-.1315	-.1266	-.2762
10.14	.9854	.8802	.4576	.4022	.1341	-.1868	-.1780	-.3673
10.18	.8820	.9623	.5034	.4209	.1533	-.2679	-.2199	-.5012
10.10	.7998	.9746	.5144	.4479	.0880	-.2961	-.2533	-.6175
10.22	.7155	1.0314	.5456	.5320	.1319	-.3887	-.3405	-.8164

RUN= 74

ALPHA	J	CP	CT	CPM	CNF	CYM	CSF	CRM
-.02	2.1387	-.4328	-.3104	.1115	.0404	-.3428	-.1761	.0383
-.02	1.7291	.0817	-.0062	.0308	-.0157	-.3407	-.1603	-.0111
.01	1.5979	.2610	.1052	-.0216	-.0579	-.3439	-.1476	-.0414
.05	1.5008	.3479	.1659	-.0486	-.0837	-.3502	-.1377	-.0626
.05	1.4114	.4983	.2348	-.0735	-.1189	-.3717	-.1682	-.1014
.05	1.3289	.5184	.2673	-.1133	-.1312	-.3735	-.1528	-.1190
.01	1.2392	.6218	.3206	-.1650	-.1775	-.3877	-.1552	-.1641
.13	1.1584	.7122	.3749	-.1718	-.1601	-.4034	-.1684	-.2151
.09	1.0651	.8069	.4256	-.2641	-.2158	-.4112	-.1429	-.2883
.09	.9702	.8807	.4758	-.3158	-.2885	-.4444	-.1416	-.3791
.09	.8806	.9745	.5280	-.3862	-.3132	-.4610	-.1223	-.5093
.16	.7966	.9888	.5428	-.4713	-.4251	-.5426	-.1762	-.6316
.09	.7074	1.0491	.5663	-.5979	-.4366	-.5509	-.1397	-.8496

TABLE AII.- Continued

RUN= 75

ALPHA	J	CP	CT	CPM	CNF	CYM	CSF	CRM
-.02	2.3117	.3181	.0756	-.1035	-.0485	-.0170	.0097	-.0241
-.02	1.8015	.8262	.2833	-.1204	-.0684	-.0099	.0089	-.1032
-.02	1.6040	1.0520	.3666	-.1366	-.0892	-.0074	.0281	-.1657
.01	1.4871	1.1774	.4247	-.1227	-.0753	-.0046	.0499	-.2158
-.02	1.4206	1.2626	.4502	-.1332	-.0644	.0162	.0444	-.2536
.01	1.3597	1.3552	.4979	-.1569	-.0995	.0390	.0656	-.2971
.05	1.2441	1.4515	.5245	-.1307	-.0509	.0693	.0705	-.3800
-.02	1.1798	1.4834	.5449	-.1457	-.0899	.0459	.0876	-.4319
.05	1.0982	1.5608	.5701	-.1686	-.0826	.0887	.1086	-.5245
.05	.9613	1.5419	.5632	-.1695	-.0796	.1258	.1636	-.6762
.09	.7797	1.5570	.5766	-.2263	-.0873	.1874	.2543	-1.0379

RUN= 77

ALPHA	J	CP	CT	CPM	CNF	CYM	CSF	CRM
-.02	2.1118	-1.0426	-.8603	-.0646	-.0144	-.1049	-.0899	.0947
-.02	1.7769	-.5188	-.4429	-.0292	.0093	-.0723	-.0653	.0666
-.02	1.5919	-.2675	-.2553	-.0518	.0038	-.0560	-.0693	.0428
-.06	1.4754	-.1447	-.1557	-.0562	-.0025	-.0312	-.0316	.0269
.05	1.4231	-.0839	-.0992	-.0425	.0022	-.0465	-.0424	.0168
.01	1.3359	-.0056	-.0335	-.0642	-.0313	-.0211	-.0267	.0013
.05	1.2132	.0952	.0469	-.0650	-.0178	-.0355	-.0311	-.0262
.09	1.1570	.1568	.0944	-.0771	-.0651	-.0016	.0043	-.0475
.01	1.0794	.2075	.1458	-.1049	-.0782	-.0091	.0054	-.0722
.05	.9749	.2930	.2114	-.0793	-.0413	.0267	.0301	-.1249
.05	.8843	.3756	.2783	-.1037	-.0492	.0445	.0552	-.1946
.05	.7944	.4125	.3152	-.1174	-.0440	.0539	.0835	-.2649
.09	.7025	.4780	.3651	-.1285	-.0541	.1208	.1498	-.3926

TABLE AII.- Continued

RUN= 92

ALPHA	J	CT	CPM	CNF	CYM	CSF	CRM
10.17	.7454	.8935	1.2691	.3359	-.3730	-.1398	.2026
10.17	.8657	.8389	1.1688	.2543	-.2463	-.0753	.1354
10.09	.9279	.8006	1.1444	.2894	-.1878	-.0528	.1083
10.25	1.0399	.7497	1.0806	.2947	-.3741	-.1439	.0809
10.06	1.1234	.6802	.9489	.2237	-.2352	-.0934	.0624
10.29	1.2116	.6557	.9118	.2290	-.1605	-.0819	.0460
10.13	1.2988	.5796	.8323	.2547	-.1582	-.0668	.0349
10.06	1.4131	.4946	.8050	.2050	-.1771	-.0508	.0295
10.06	1.5061	.4398	.7420	.2014	-.1462	-.0305	.0296
10.02	1.5940	.3910	.6854	.1685	-.1124	-.0174	.0269
10.02	1.6531	.3816	.7188	.2591	-.1870	-.0370	.0249
10.02	1.7481	.3526	.6647	.2021	-.1450	-.0289	.0224
10.02	1.8686	.3305	.6834	.2236	-.0758	-.0199	.0225

RUN= 93

ALPHA	J	CT	CPM	CNF	CYM	CSF	CRM
20.23	.7433	.9080	2.4123	.7380	-.1853	-.0698	.1890
20.11	.8491	.8555	2.1562	.6268	-.1901	-.0725	.1291
20.03	.9318	.8075	2.1033	.6702	-.2097	-.0907	.1099
20.03	1.0320	.7624	1.9118	.6413	-.0767	.0090	.0815
20.03	1.1227	.7069	1.7404	.5691	-.0208	-.0030	.0596
20.07	1.2089	.6710	1.6263	.5324	.0396	.0374	.0428
20.03	1.2983	.6243	1.5521	.5129	.0432	.0554	.0370
20.03	1.3956	.5564	1.4194	.4493	.0116	.0242	.0274
20.07	1.4683	.5123	1.3853	.4640	.0511	.0570	.0256
19.98	1.6075	.4618	1.2963	.4436	.0733	.0456	.0197
19.98	1.6709	.4396	1.2228	.3729	.0495	.0518	.0217
20.03	1.7867	.4315	1.1620	.3863	-.0059	.0196	.0157
20.03	1.8367	.4423	1.1793	.3884	.0247	.0418	.0160

TABLE AII.- Continued

RUN=106

ALPHA	J	CT	CPM	CNF	CYM	CSF	CRM
.03	.7785	1.2599	-.6199	-.3710	.0106	-.0629	.2592
-.01	.8302	1.2247	-.7004	-.4002	.0521	-.0415	.2125
.03	.9346	1.1277	-.4155	-.2454	.0255	-.0082	.1499
-.01	1.0145	1.0694	-.4683	-.2813	-.1395	-.0983	.1236
.03	1.1323	.9691	-.3732	-.2010	-.0566	-.0402	.0815
.03	1.1263	.9660	-.3899	-.2168	.0049	-.0311	.0816
.03	1.2599	.8441	-.3540	-.2352	-.0200	-.0152	.0627
-.01	1.4124	.6923	-.3350	-.2115	-.0140	-.0212	.0441
.03	1.4964	.6025	-.3193	-.1757	-.0162	-.0241	.0364
-.01	1.5993	.5191	-.3058	-.1703	-.0098	-.0267	.0283
.03	1.6609	.4904	-.3126	-.1787	-.0477	-.0306	.0282
-.01	1.8079	.3997	-.2511	-.1273	-.0378	-.0347	.0231
-.01	1.9193	.3393	-.2867	-.1404	-.0400	-.0126	.0223

RUN=112

ALPHA	J	CT	CPM	CNF	CYM	CSF	CRM
-.01	.7682	.8331	-.4398	-.3991	-.0331	-.0321	.1609
-.01	.8401	.7870	-.4449	-.4062	-.0469	-.0503	.1161
-.04	.9310	.7339	-.4452	-.4107	-.0424	-.0108	.0939
-.04	1.0090	.6924	-.3590	-.3045	-.0101	-.0171	.0599
-.04	1.0986	.6427	-.3415	-.2831	-.0198	-.0191	.0489
-.04	1.2263	.5628	-.2672	-.1853	.0046	-.0104	.0261
-.01	1.3082	.5045	-.2792	-.2118	-.1164	-.0506	.0251
-.04	1.4047	.4350	-.2181	-.1952	-.0790	-.0239	.0218
-.04	1.4912	.3690	-.2001	-.2004	-.0300	-.0095	.0154
-.04	1.5933	.2794	-.2652	-.2088	-.0118	.0048	.0121
-.08	1.6722	.1991	-.2387	-.1985	-.0318	-.0268	.0094
-.08	1.7751	.1149	-.1653	-.1532	-.0061	.0057	.0085
-.04	1.8739	.0822	-.2177	-.1831	-.0278	.0061	.0099

TABLE AII.- Continued

RUN=119

ALPHA	J	CT	CYM	CSF
.13	.7410	.8576	-.0603	-.0740
.05	.8515	.7989	-.0673	-.0573
-.02	.9429	.7450	-.1159	-.1495
.02	1.0280	.7140	-.0624	-.0740
-.02	1.1364	.6198	-.0852	-.1259
.02	1.2200	.5604	-.0884	-.1125
-.02	1.3129	.4822	-.0706	-.0677
-.02	1.4083	.4170	-.0612	-.0735
-.02	1.4999	.3943	-.1170	-.2243
-.02	1.5922	.2872	-.1090	-.1354
-.02	1.6586	.2277	-.0960	-.1231
-.06	1.7908	.1210	-.0673	-.0905
-.06	1.8600	.0695	-.0610	-.1001

RUN=120 (NOTE MODEL AT PSI=10 DEGREES IN WIND TUNNEL. ALPHA FOR PYLON =10 DEGREES)

ALPHA	J	CT	CYM	CSF
.13	.7377	.8701	-.2958	-1.2836
.05	.8451	.8151	-.3355	-1.2151
-.02	.9404	.7710	-.3775	-1.2627
.02	1.0295	.6771	-.3810	-1.1413
-.02	1.1332	.6523	-.4038	-1.0820
.02	1.2021	.6064	-.4113	-1.0711
-.02	1.3183	.5447	-.4587	-1.0648
-.02	1.4147	.4766	-.4576	-1.0282
-.02	1.4962	.4292	-.4824	-1.0385
-.02	1.5954	.3812	-.4966	-1.0132
-.02	1.6755	.3279	-.4983	-1.0157
-.06	1.7905	.2298	-.4859	-.9598
-.06	1.8772	.1925	-.5013	-.9436

TABLE AII.- Continued

RUN=127

ALPHA	J	CT	CYM	CSF
.05	.7378	.3147	-.0522	-.1296
.05	.8836	.2970	-.0104	-.0631
.05	.9517	.2765	-.0322	-.0711
.05	1.0281	.3793	-.0663	-.1152
.02	1.1243	.2166	-.0568	-.1210
.02	1.2150	.1856	-.0461	-.0890
.02	1.3230	.1443	-.0469	-.0880
.02	1.4200	.1089	-.0729	-.1296
.02	1.4987	.0588	-.1385	-.2350
.02	1.6064	.0350	-.0780	-.1351
.02	1.6657	.0056	-.0453	-.0885
.02	1.7848	-.0622	-.0675	-.1148
.02	1.8921	-.1284	-.0426	-.0903

RUN=128

ALPHA	J	CT	CYM	CSF
.13	.7393	.5036	-.0856	-.1270
.09	.8667	.4749	.0013	-.0156
.05	.9520	.4409	-.0532	-.1168
.09	1.0306	.4811	-.0480	-.1103
.05	1.1036	.3800	-.0686	-.1019
.05	1.2223	.3261	-.0605	-.1310
.05	1.3110	.2899	-.0333	-.0667
.05	1.4037	.2379	-.0514	-.1011
.02	1.4884	.2113	-.1290	-.2622
.02	1.5798	.1421	-.0527	-.1236
.02	1.6534	.0954	-.0736	-.1291
.02	1.7983	.0101	-.0397	-.0818
-.02	1.8747	-.0570	-.0938	-.1735

TABLE AII.- Concluded

RUN=129

ALPHA	J	CT	CYM	CSF
.13	.7753	1.2481	-.0463	-.1243
.13	.8483	1.1938	-.0788	-.0297
.13	.9671	1.0923	-.0417	-.0084
.13	1.0457	1.0225	-.0517	-.0759
.09	1.1353	.9451	-.0824	-.0847
.13	1.1218	.9549	-.0510	-.0679
.09	1.2037	.8626	-.0390	-.0406
.09	1.2586	.7988	-.0487	-.0281
.05	1.4369	.6191	-.0377	-.0512
.05	1.5165	.5157	-.0363	-.0314
.05	1.6097	.4099	-.0808	-.1064
.02	1.6860	.3135	-.0671	-.0962
.02	1.8073	.1776	-.0591	-.0814
.02	1.8986	.0564	-.0982	-.1688

REFERENCES

1. Goldsmith, I. M.: A Study To Define the Research and Technology Requirements for Advanced Turbo/Propfan Transport Aircraft. NASA CR-166138, 1981.

2. Jeracki, Robert J.; Mikkelson, Daniel C.; and Blaha, Bernard J.: Wind Tunnel Performance of Four Energy Efficient Propellers Designed for Mach 0.8 Cruise. NASA TM-79124, 1979. (Available as SAE Paper 790573.)

3. Sellers, William L., III; and Elliott, Joe W.: Recent Applications of a Laser Velocimeter in the Langley 4- by 7-Meter Wind Tunnel. NASA paper presented at 8th Biennial Symposium on Turbulence, Univ. of Missouri-Rolla, Sept. 1983.

4. Coe, Paul L., Jr.; Applin, Zachary T.; and Williams, Louis J.: Stability and Control Results for Advanced Turboprop Aft-Mount Installations. SAE 1984 Transactions, Volume 93, Soc. Automot. Eng., Inc., c.1985, pp. 6.256-6.263. (Available as 841479.)

5. Ridder, Sven-Olof: Wind Tunnel Test of a Twin, Rear Propeller Transport Aircraft Configuration at Low Speeds. ICAS Proceedings 1984 - 14th Congress of the International Council of the Aeronautical Sciences, Volume 2, B. Laschka and R. Staufenbiel, eds., International Council of Aeronautical Sciences, c.1984, pp. 644-654. (Available as ICAS-84-2.6.3.)

6. Aljabri, A. S.; and Hughes, A. C.: Wind Tunnel Investigation of the Interaction of Propeller Slipstream With Nacelle/Wing/Flap Combinations. Aerodynamics and Acoustics of Propellers, AGARD-CP-366, Feb. 1985, pp. 21-1 - 21-10.

TABLE I.- NACELLE ORDINATES

(a) Forward-nacelle ordinates

x, in.	r, in., for -	
	SR propeller	CR propeller
-6.028		0
-6.000		.149
-5.500		.525
-5.000		.857
-4.500		1.140
-4.000		1.405
-3.500		1.638
-3.000		1.845
-2.500		2.015
-2.000		2.145
-1.500		2.235
-1.250		2.250
0	0	2.250
.270	.340	↓
.440	.480	
.780	.710	
1.110	.920	
1.810	1.230	
2.510	1.500	
3.220	1.730	2.250
3.890	1.870	2.333
4.640	1.930	2.545
5.040	2.020	2.685
5.600	2.210	2.840
6.230	2.450	2.935
6.600	2.580	2.970
6.617	2.581	2.976
6.738	2.619	2.982
6.876	2.665	2.986
7.014	2.707	3.000
7.152	2.745	↓
7.290	2.778	
7.703	2.859	
8.393	2.945	
9.428	2.997	
10.000	3.000	
.	↓	
.		
.		
28.000		

(b) Aft-nacelle ordinates

x, in.	r, in., for -	
	Sting adapter	Aft fairing
28.000	3.000	3.000
29.000	3.000	3.000
30.000	2.940	2.960
31.000	2.900	2.891
32.000	2.850	2.730
33.000	2.520	2.550
34.000	2.300	2.290
35.000	2.160	1.945
36.000	2.020	1.500
37.000	1.920	.861
37.717	1.831	0
38.000	1.820	
39.000	1.750	
40.000	1.680	
41.000	1.620	
42.000	1.600	
43.000	1.560	
43.317	1.550	

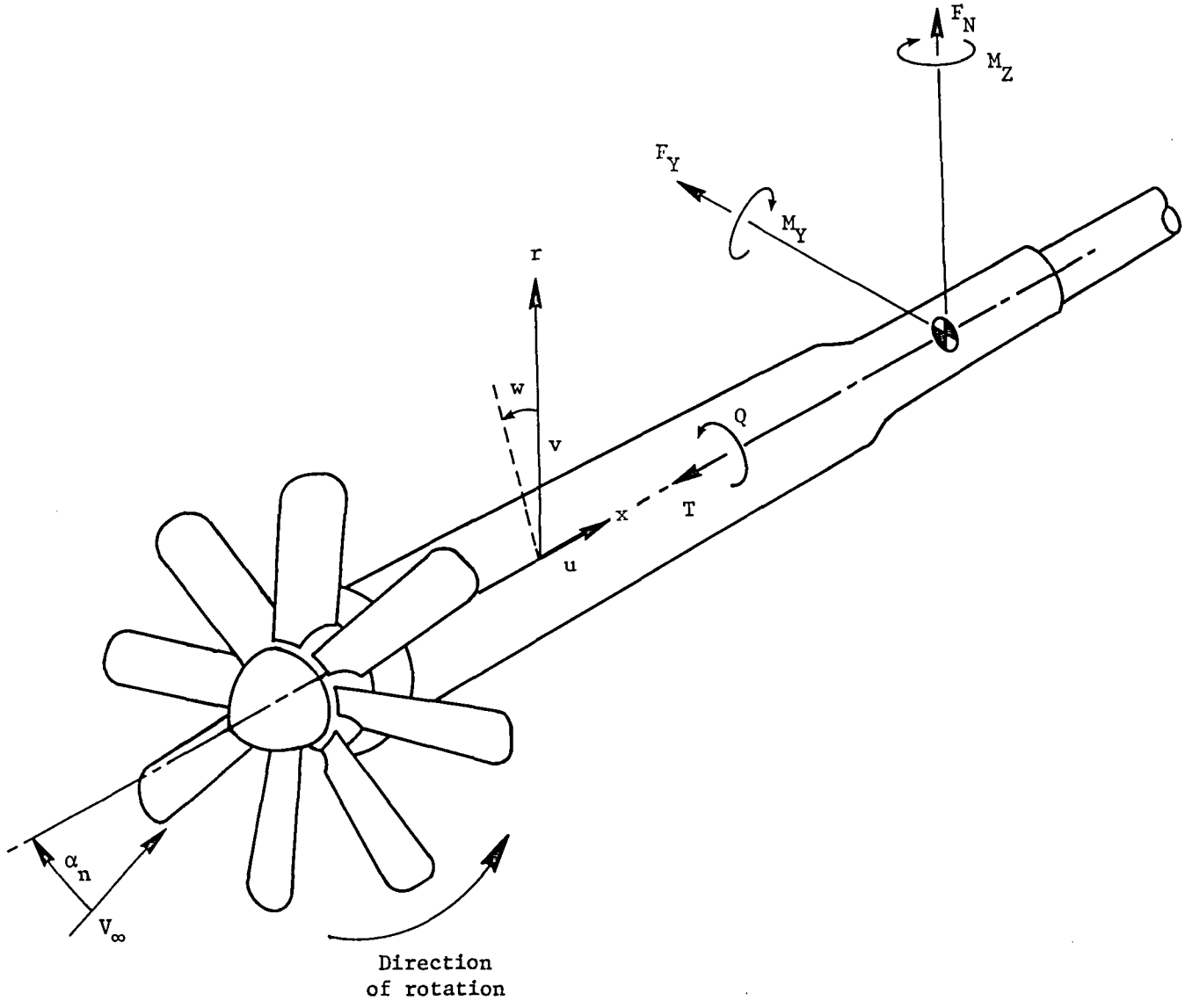

Figure 1.- Sketch of propeller and nacelle showing body system of axes.

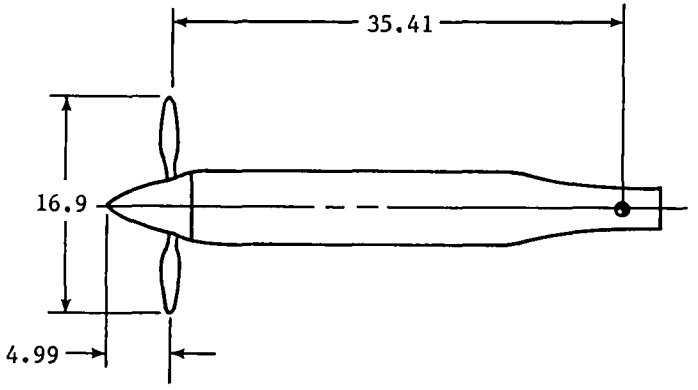

(a) SRT,S.

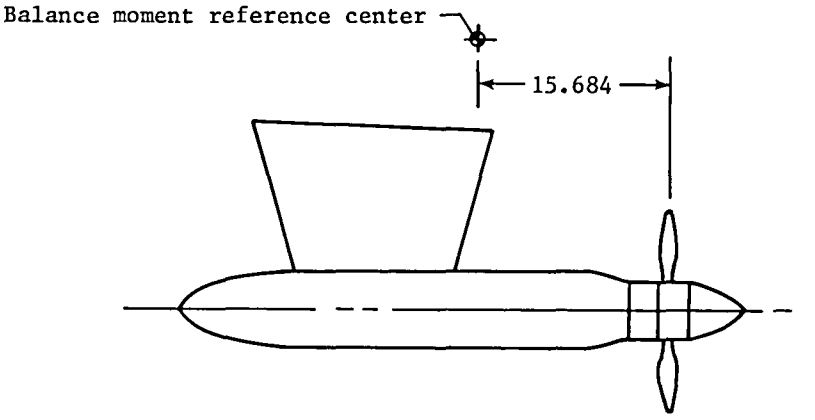

(b) SRP,P.

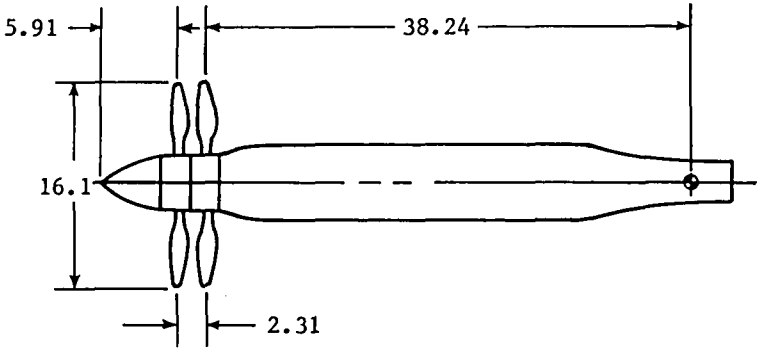

(c) CRT,S.

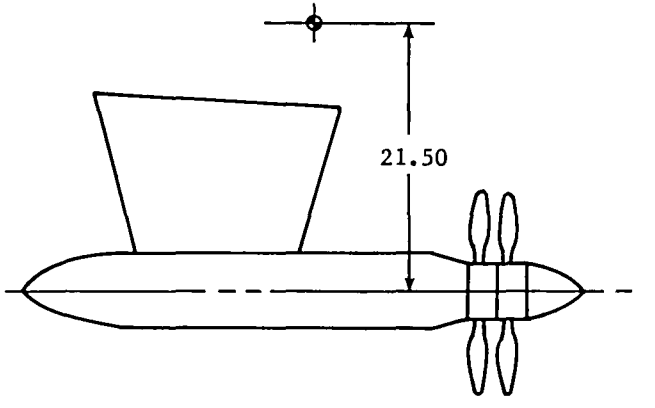

(d) CRP,P.

Figure 2.- Propeller/nacelle mounting arrangements. Dimensions are given in inches.

L-86-308

Figure 3.- Photograph of pylon-mounted pusher propeller/nacelle.

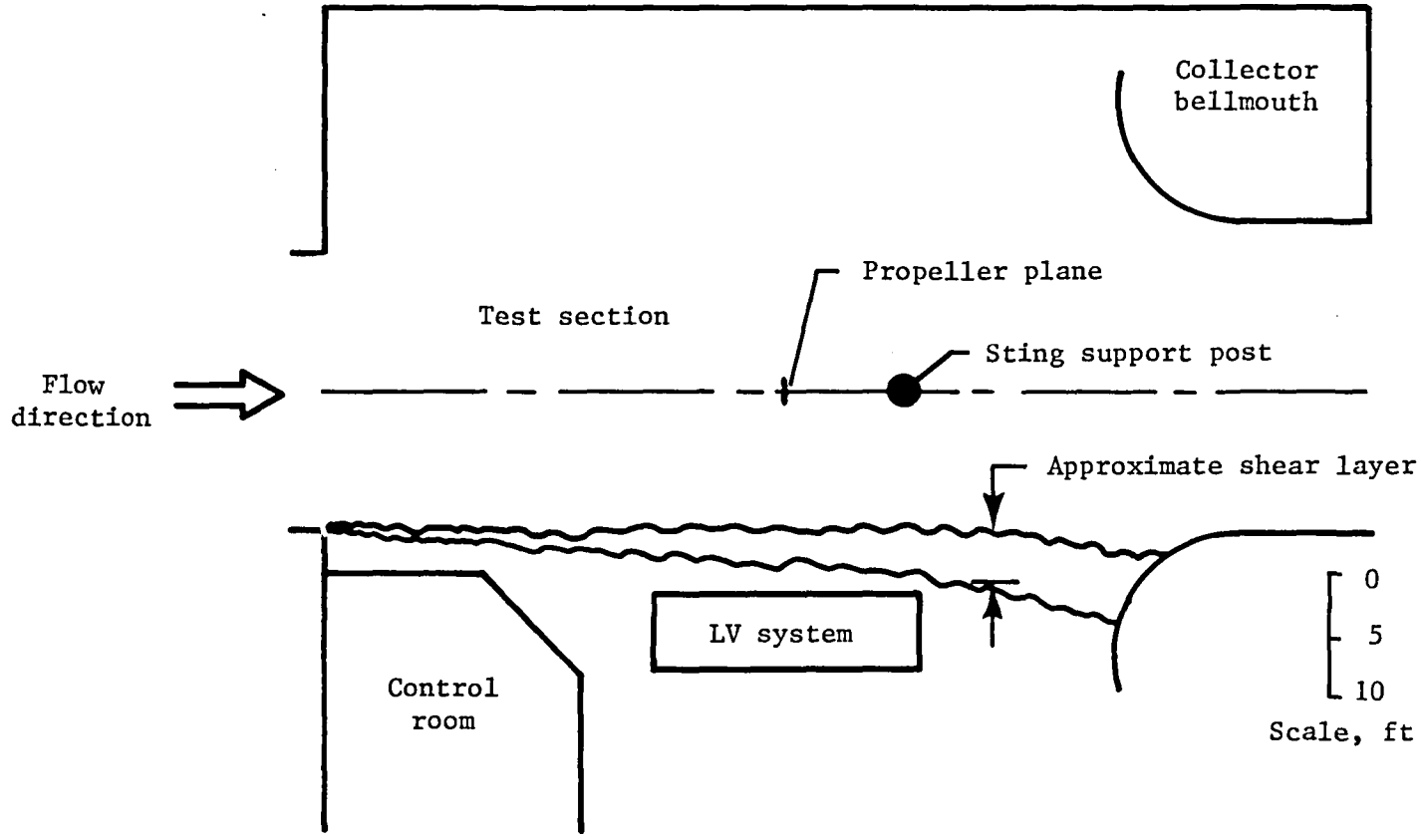

Figure 4.- Plan view of Langley 4- by 7-Meter Tunnel.

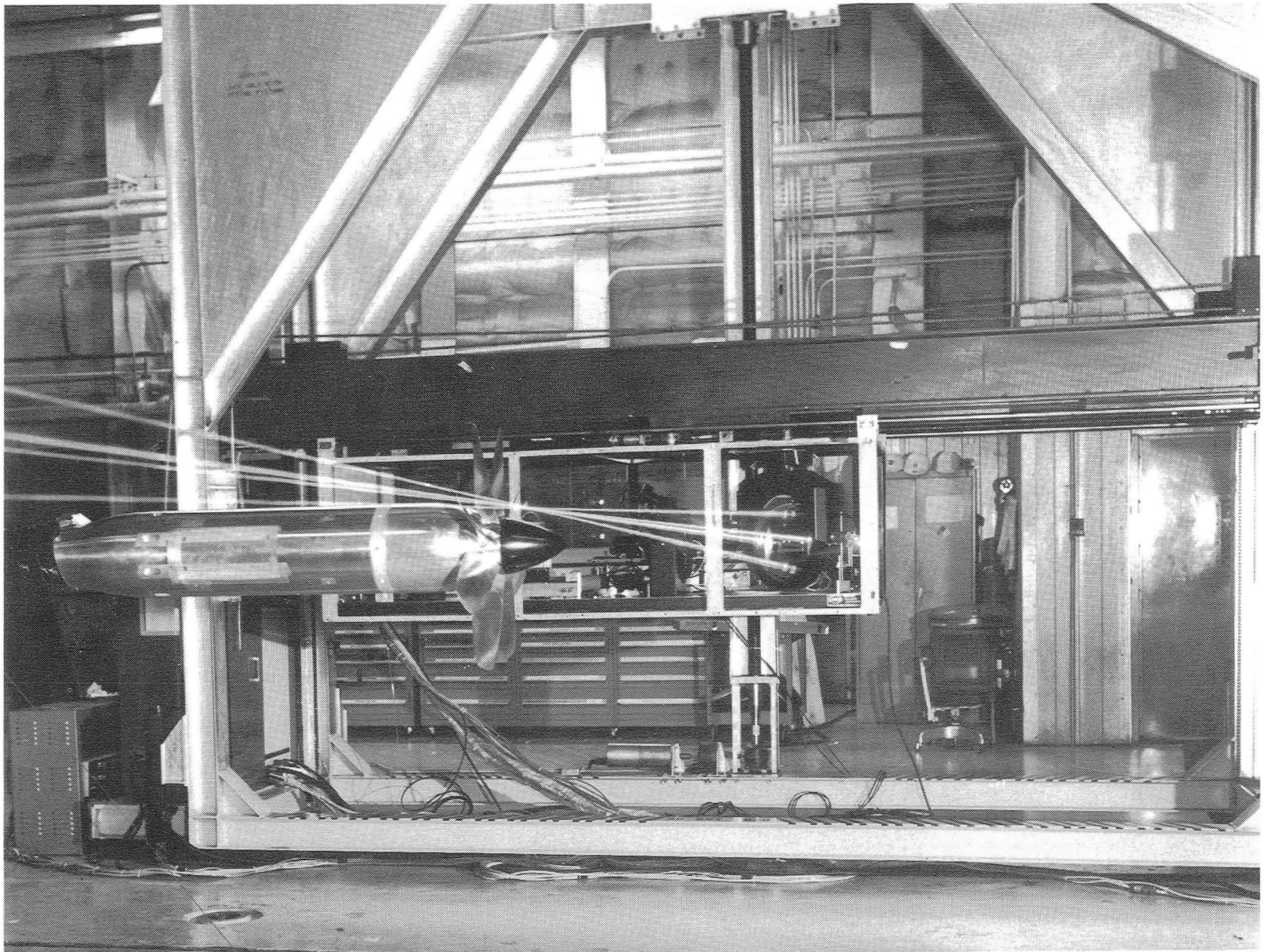

L-83-4023

Figure 5.- LV system in the Langley 4- by 7-Meter Tunnel.

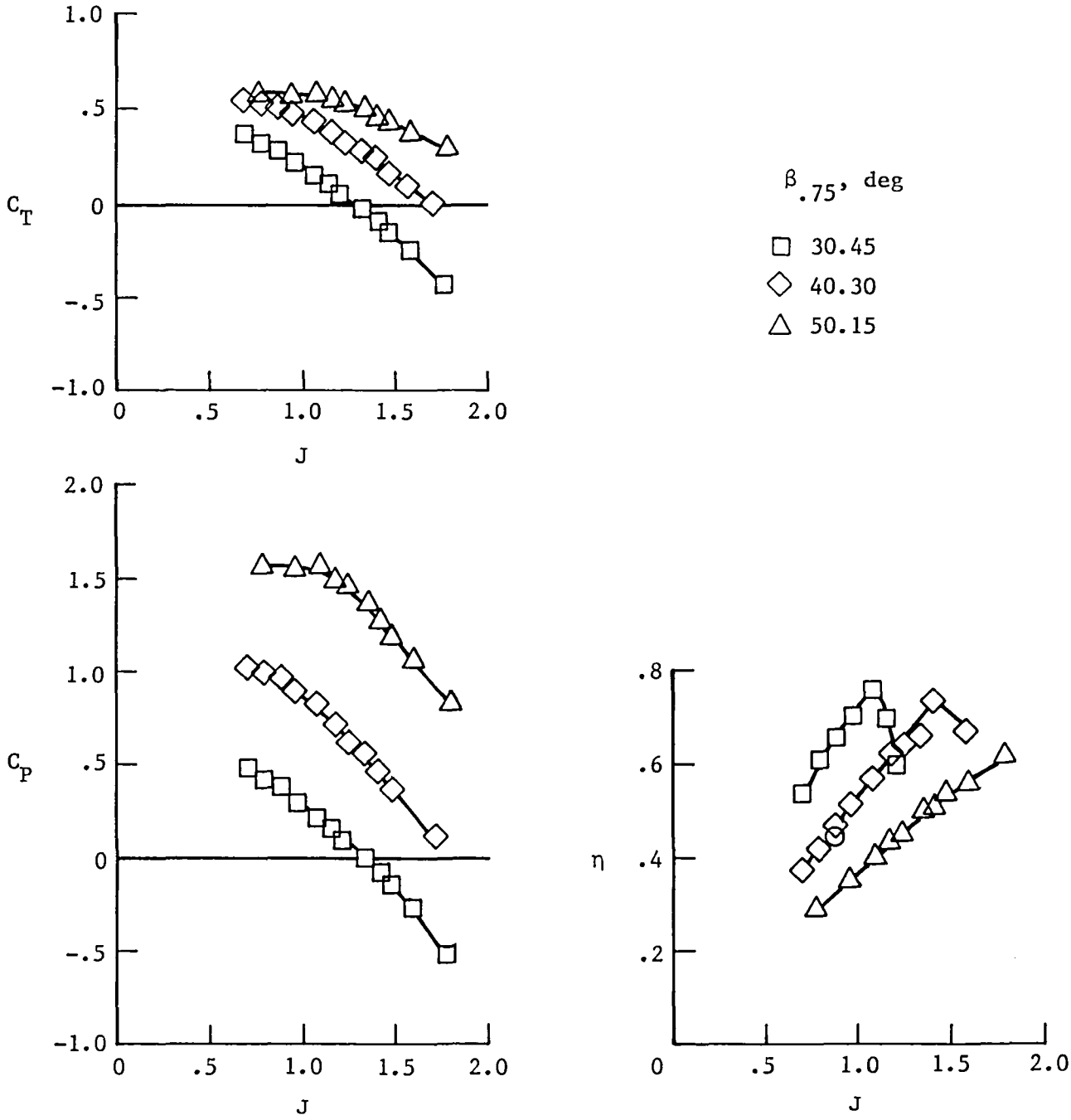

Figure 6.- Effect of blade angle on performance of eight-blade single-rotation propeller.

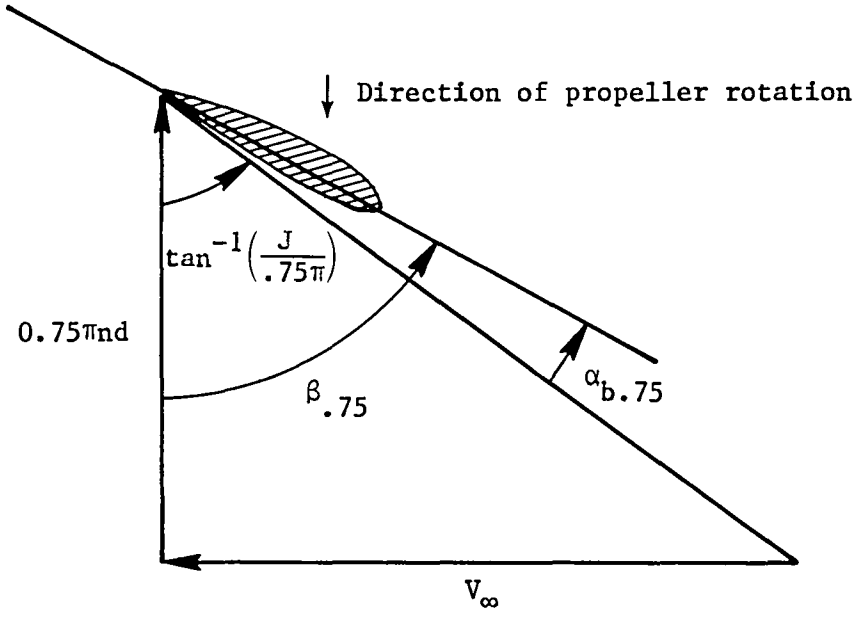

Figure 7.- Relationship between $\alpha_{b.75}$, $\beta_{.75}$, and advance ratio J. For nacelle angle of attack α_n of 0°, $\alpha_{b.75} = \beta_{.75} - \tan^{-1}\left(\frac{J}{0.75\pi}\right)$.

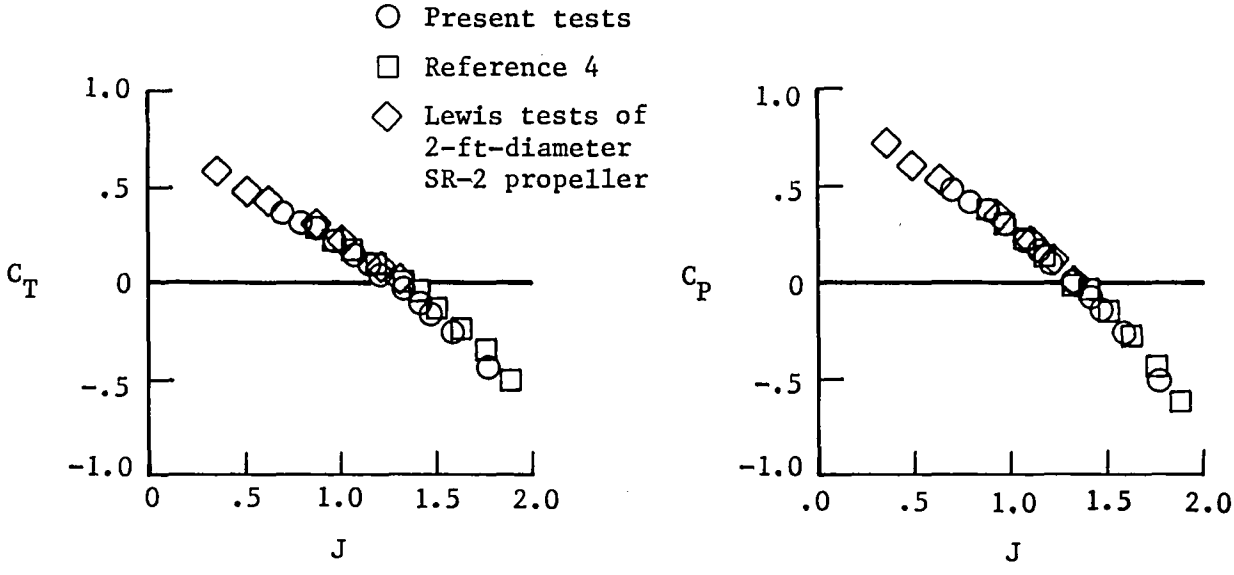

Figure 8.- Comparison of single-rotation performance data from present tests with prior tests. $\beta_{.75} \approx 30°$.

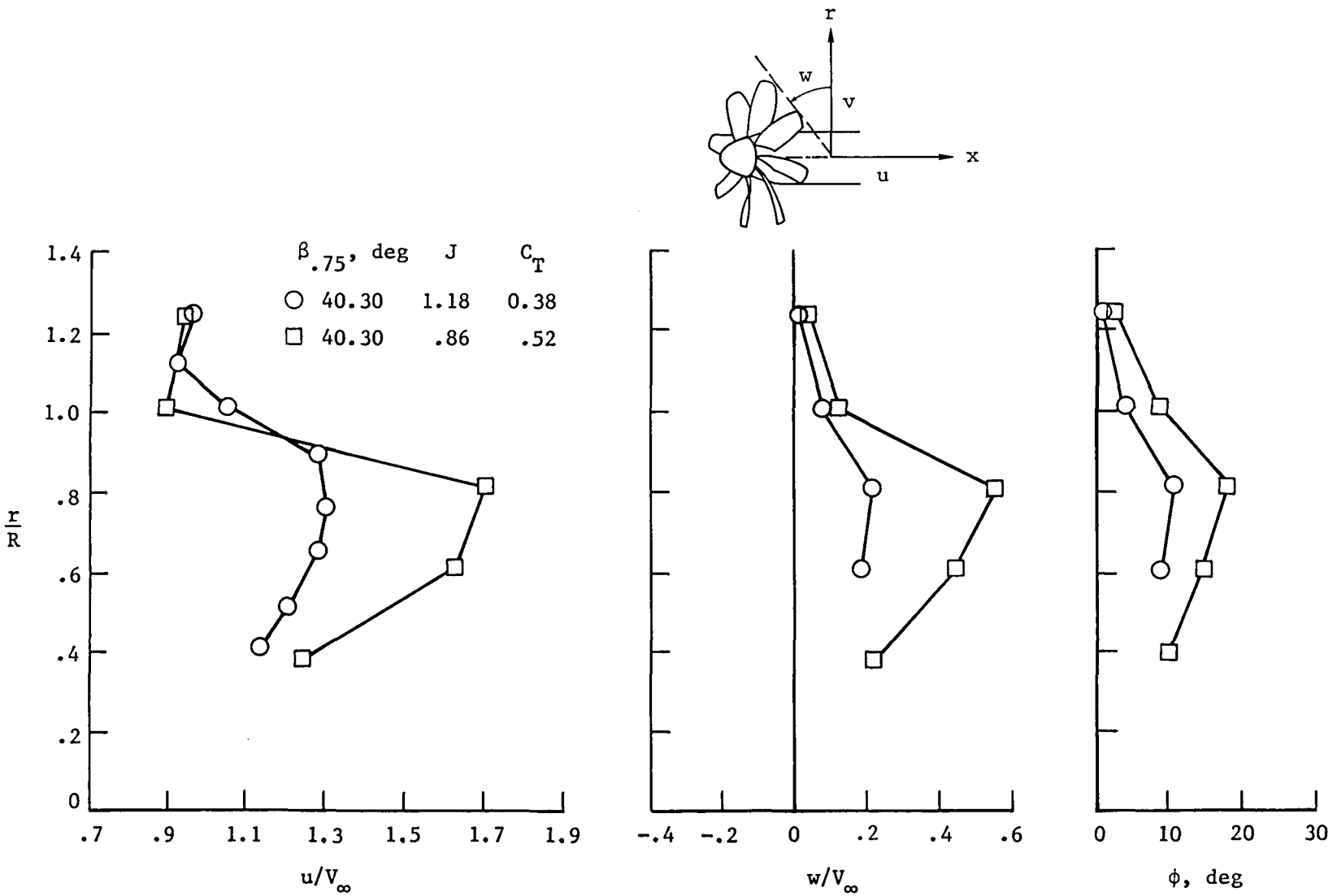

Figure 9.- Effect of advance ratio on flow field behind single-rotation propeller. Measured 1.25 in. behind pitch change axis.

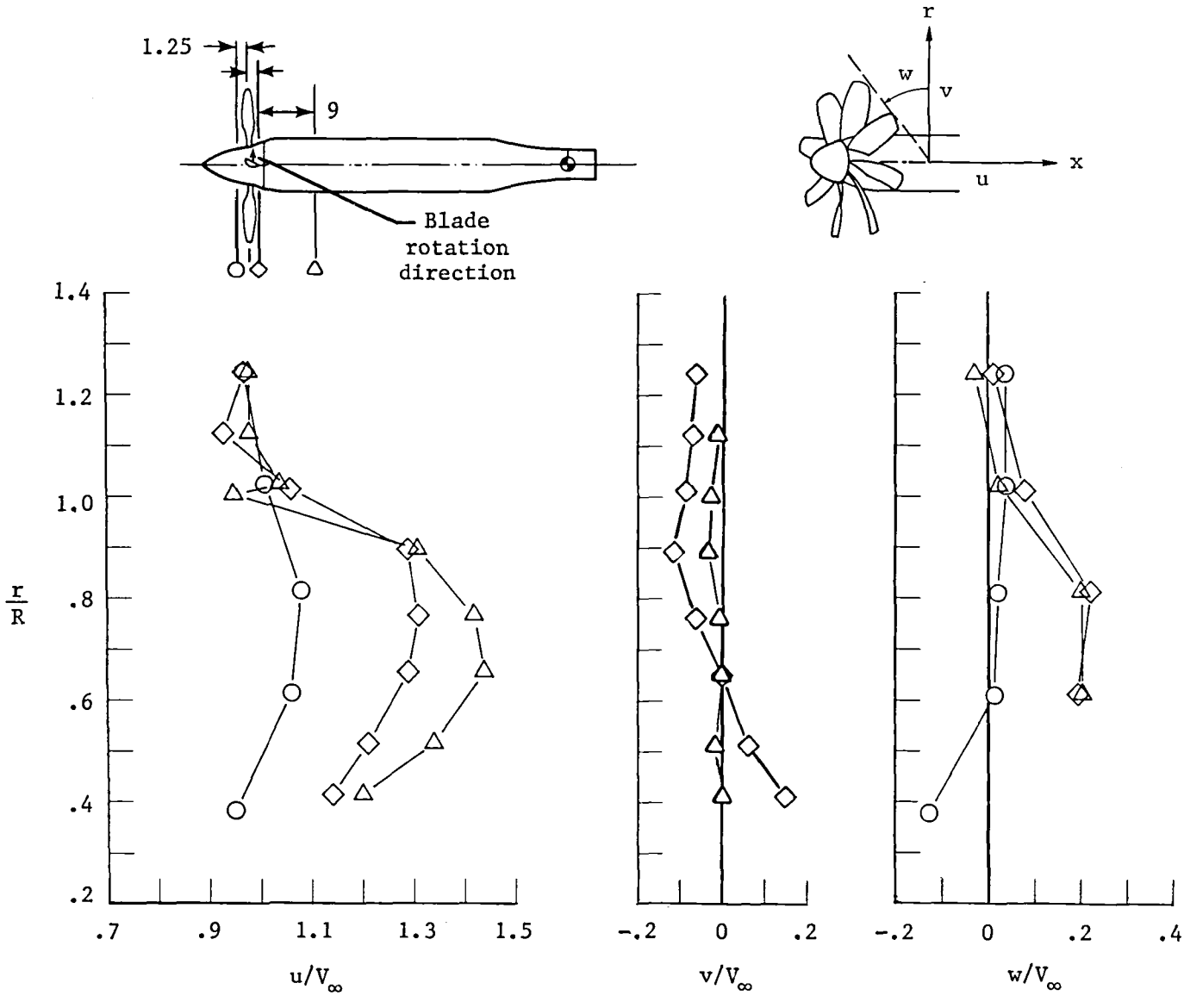

Figure 10.- Propeller flow-field velocity ratios for single-rotation tractor configuration. $\beta_{.75}$ = 40.30°; J = 1.18; C_T = 0.38. Dimensions are given in inches.

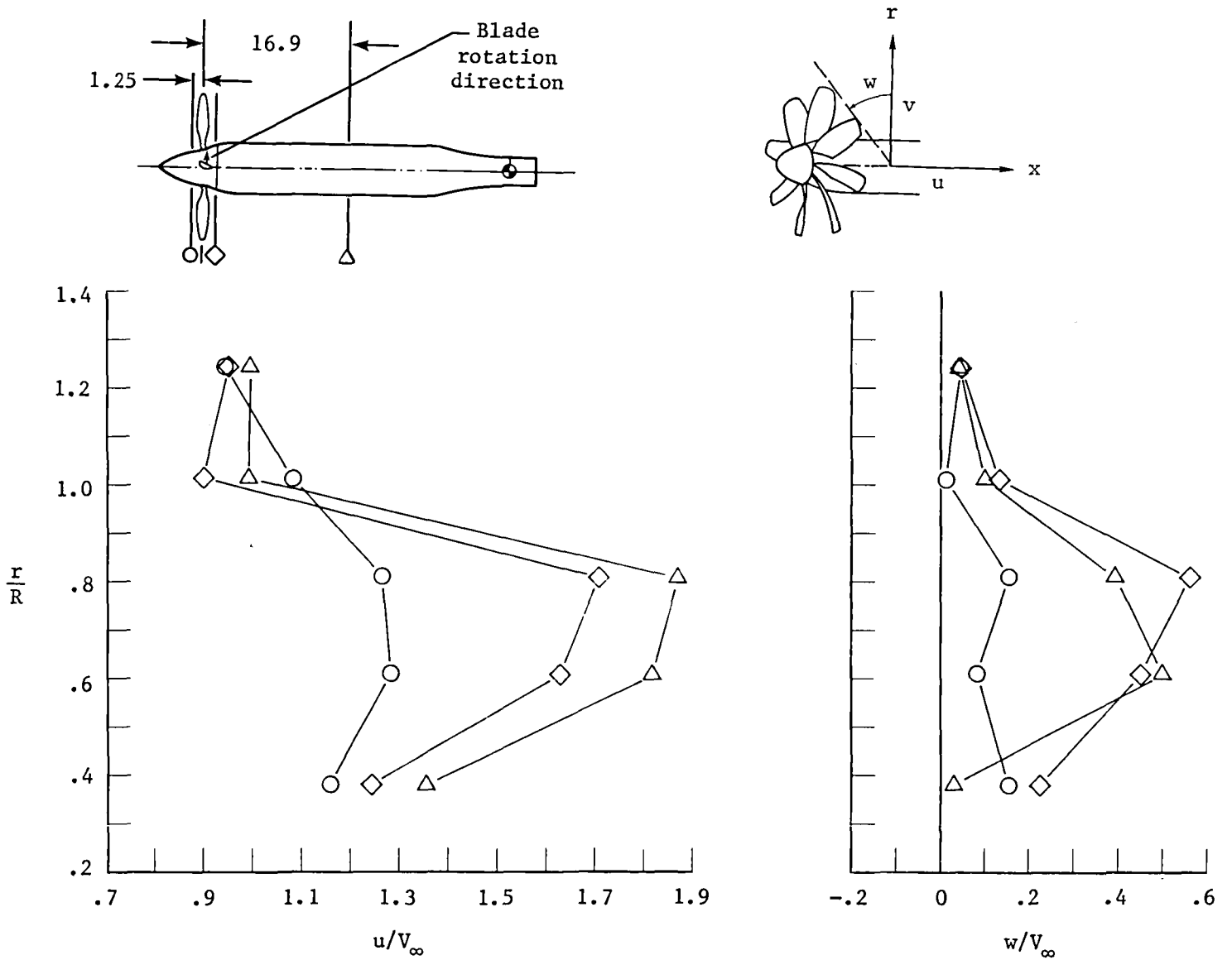

Figure 11.- Propeller flow-field velocity ratios for single-rotation tractor configuration. $\beta_{.75}$ = 40.30°; J = 0.86; C_T = 0.52. Dimensions are given in inches.

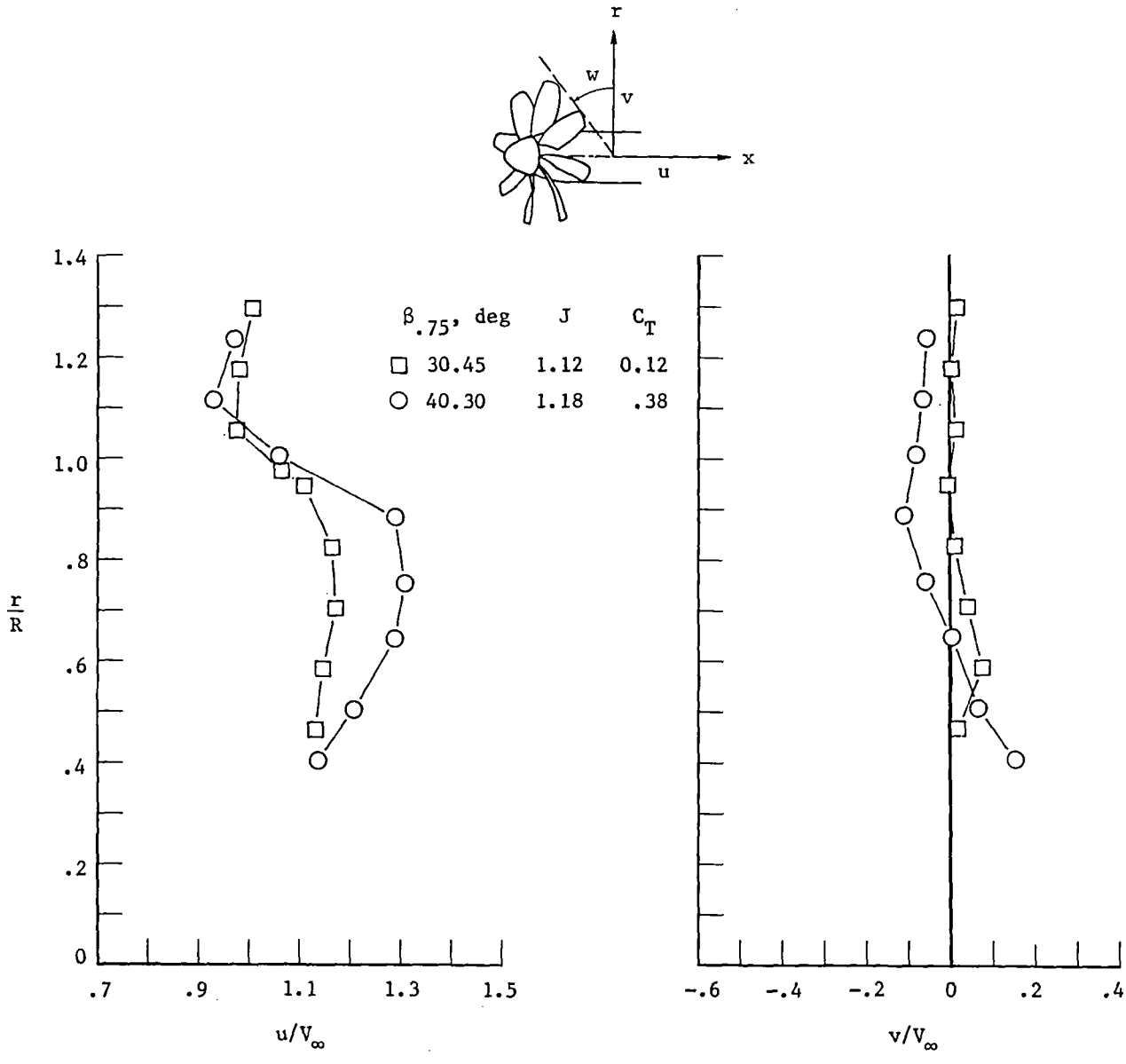

Figure 12.- Effect of blade angle on flow field behind single-rotation tractor propeller/nacelle. Measured 1.25 in. behind pitch change axis.

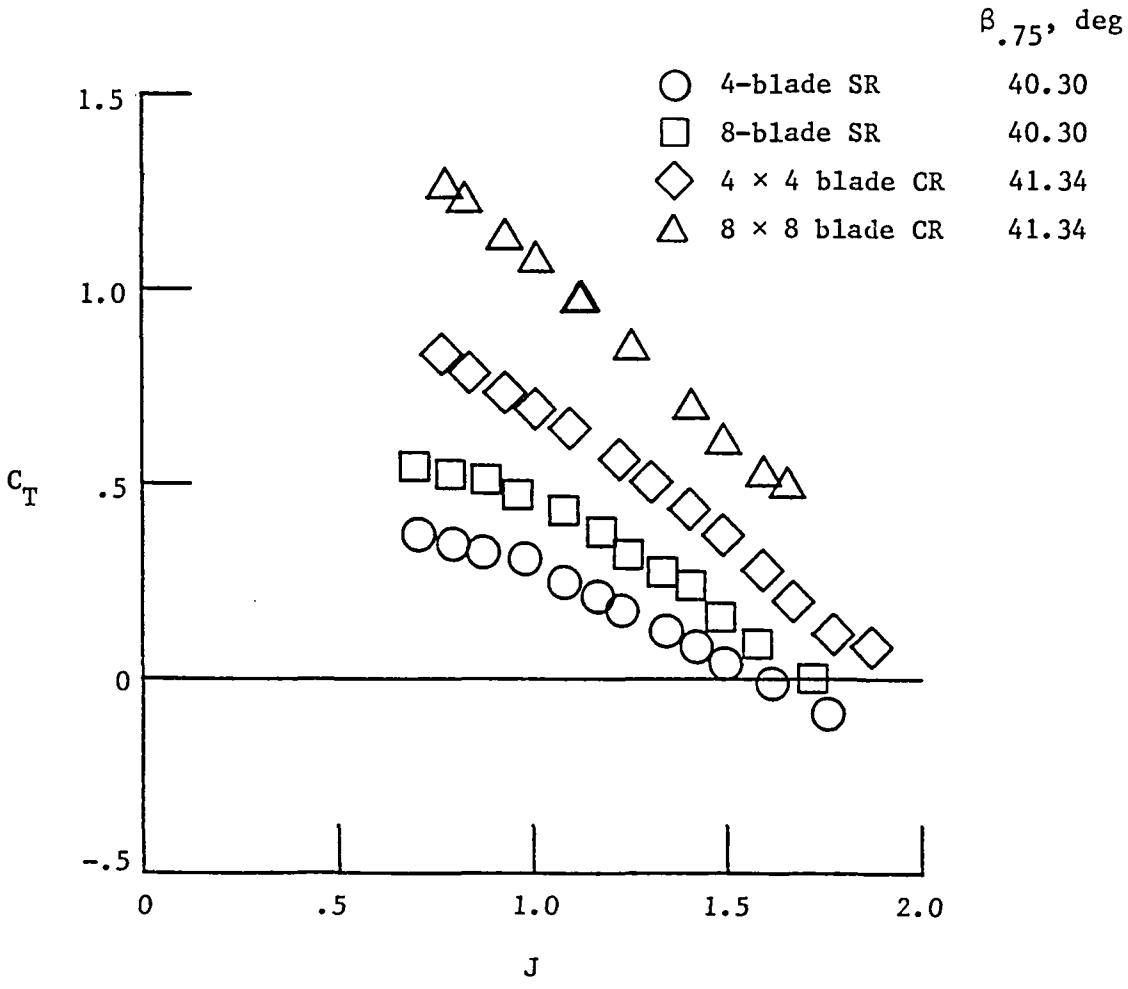

Figure 13.- Variation of thrust coefficient with advance ratio for single- and counter-rotation tractor propellers.

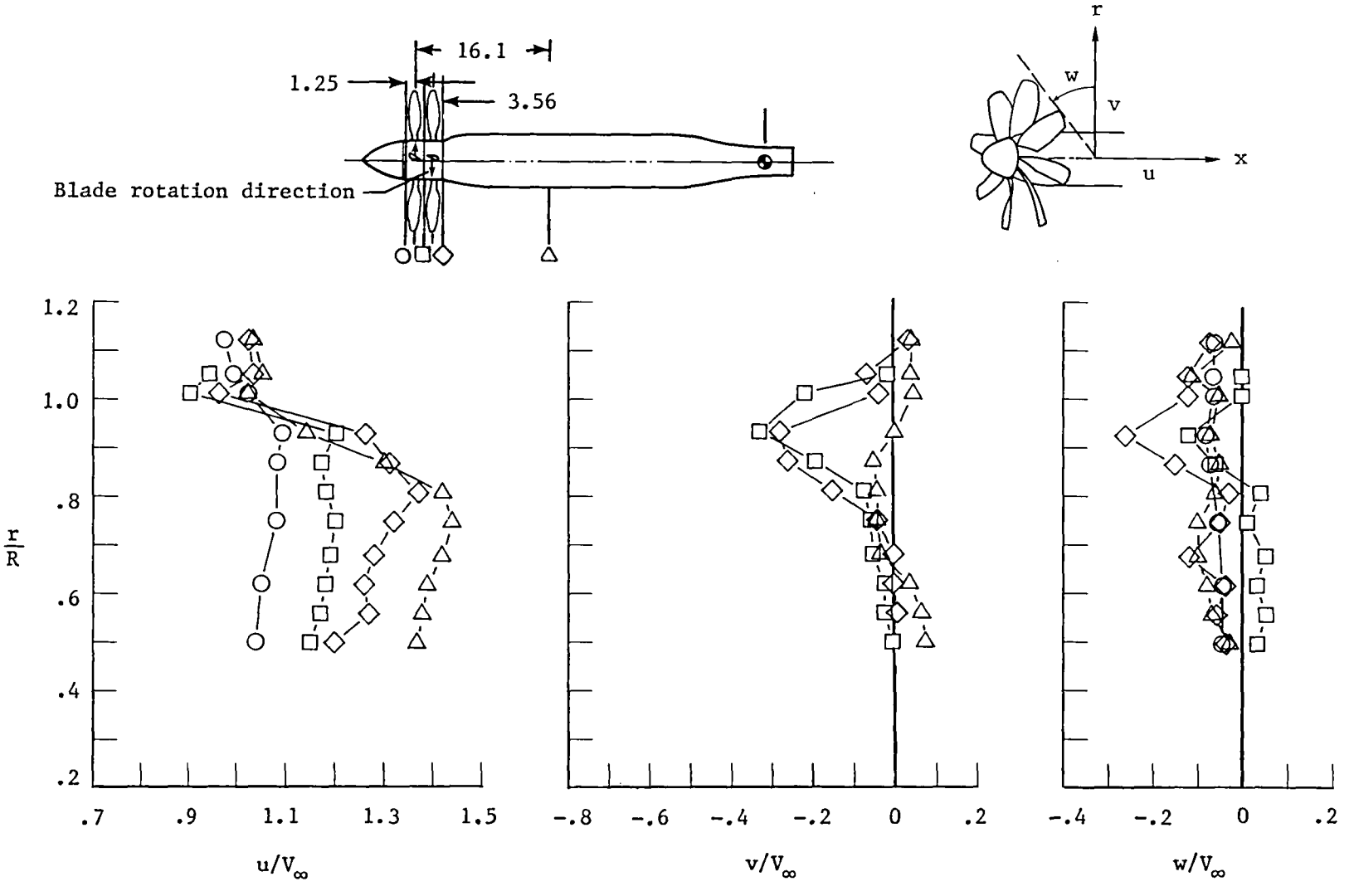

Figure 14.- Propeller flow-field velocity ratios for counter-rotation tractor configuration. $\beta_{.75}$ = 41.34°/41.34°; J = 1.21; C_T = 0.56. Dimensions are given in inches.

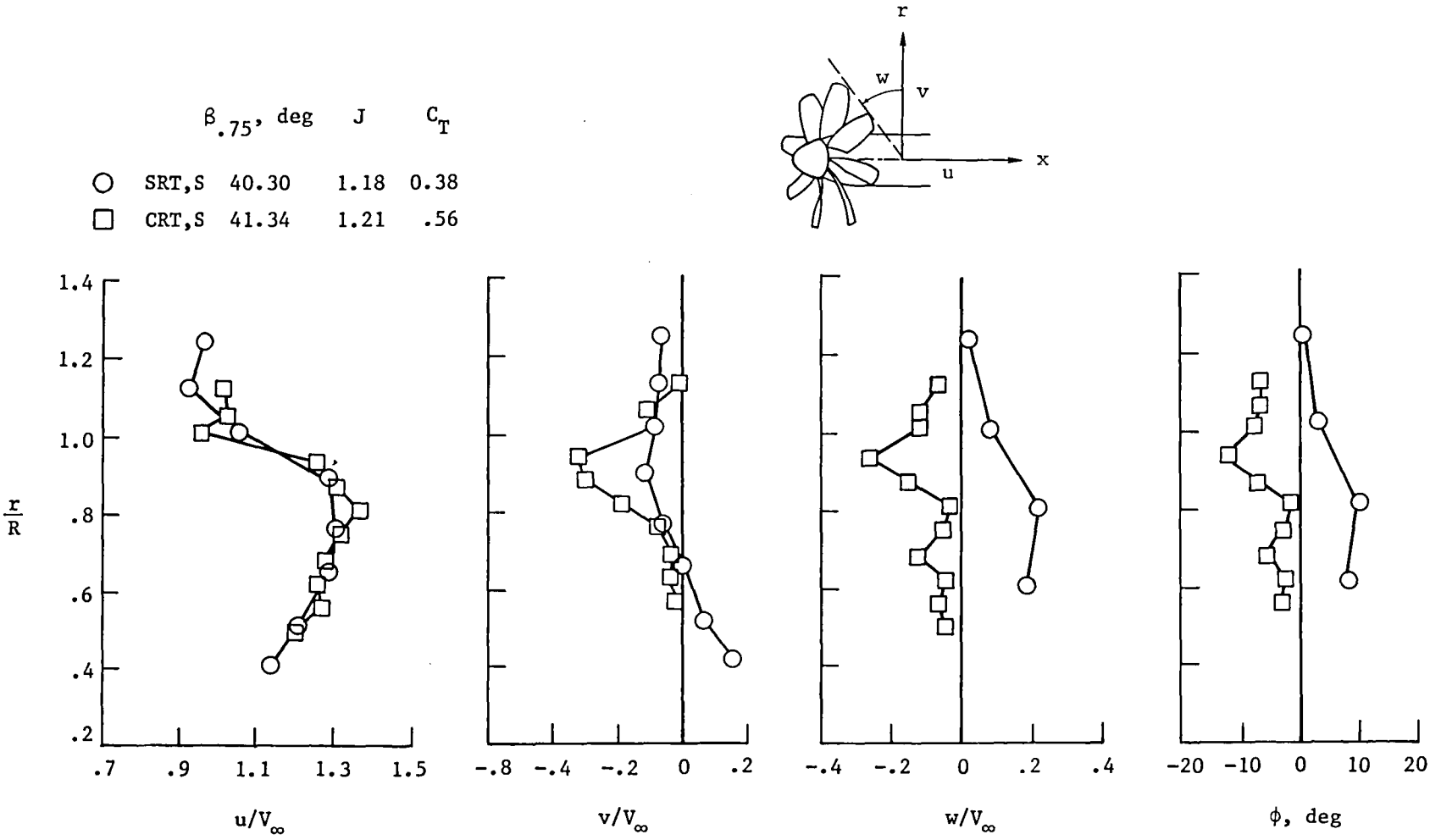

Figure 15.- Comparison of propeller flow fields measured 1.25 in. behind single-rotation propeller pitch change axis and 1.25 in. behind counter-rotation rear-propeller pitch change axis.

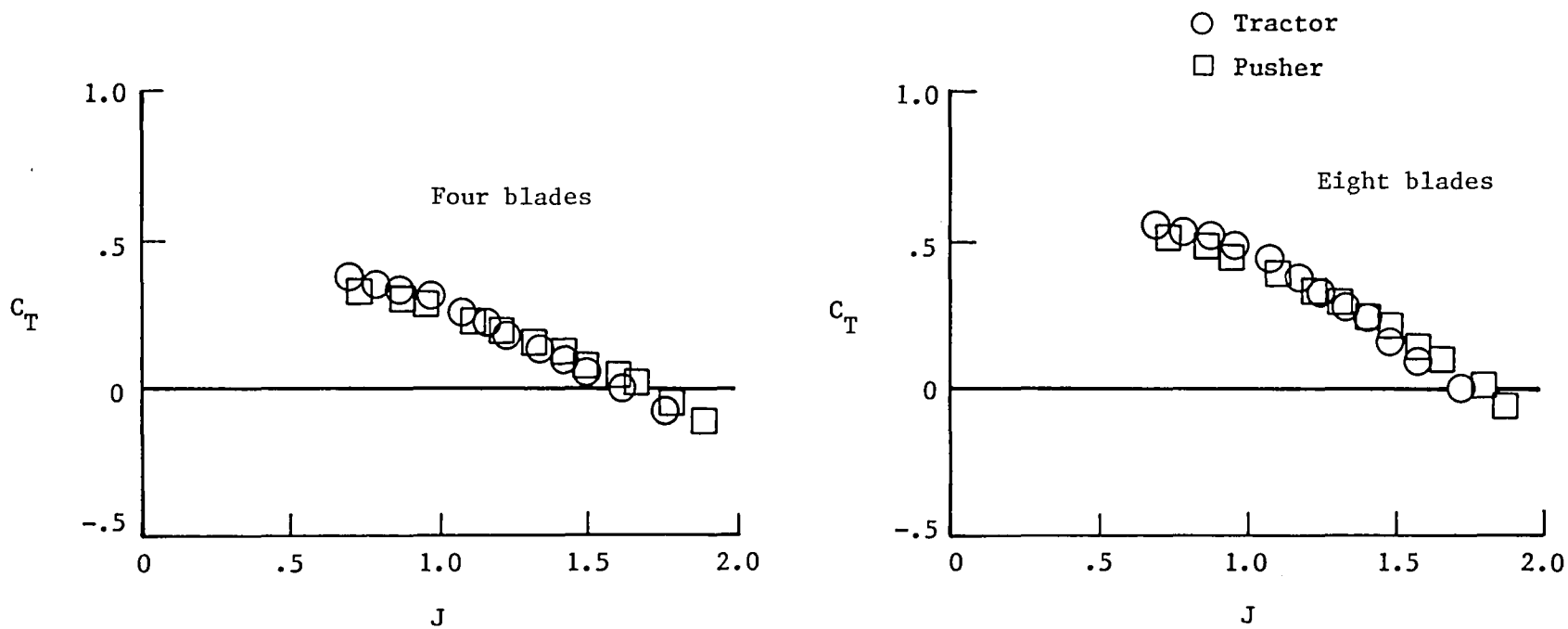

(a) Single-rotation propeller. $\beta_{.75} = 40.30°$.

Figure 16.- Comparison of thrust coefficient plotted against advance ratio for tractor and pusher propellers. $\alpha_n = 0°$.

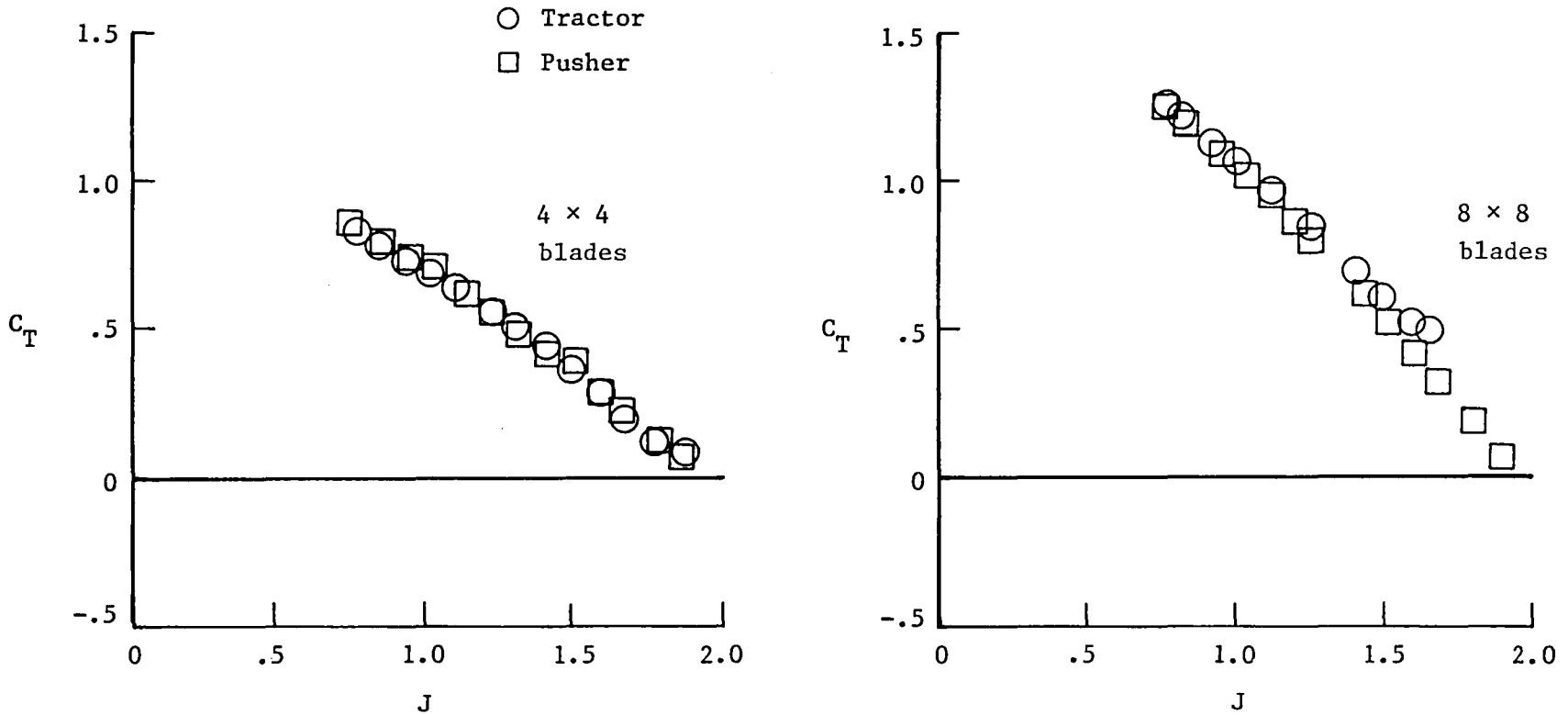

(b) Counter-rotation propeller. $\beta_{.75}$ = 41.34°/41.34°.

Figure 16.- Concluded.

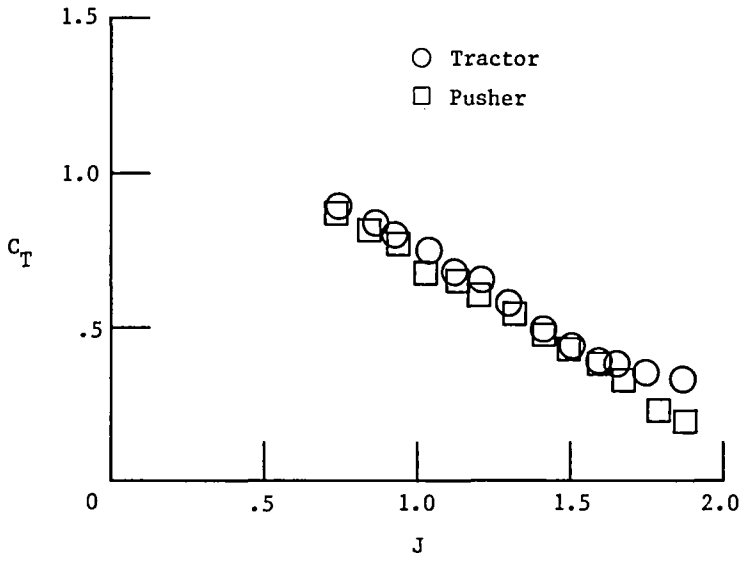

Figure 17.- Comparison of thrust coefficient plotted against advance ratio for 4 × 4 counter-rotation tractor and pusher propellers. α_n = 10°.

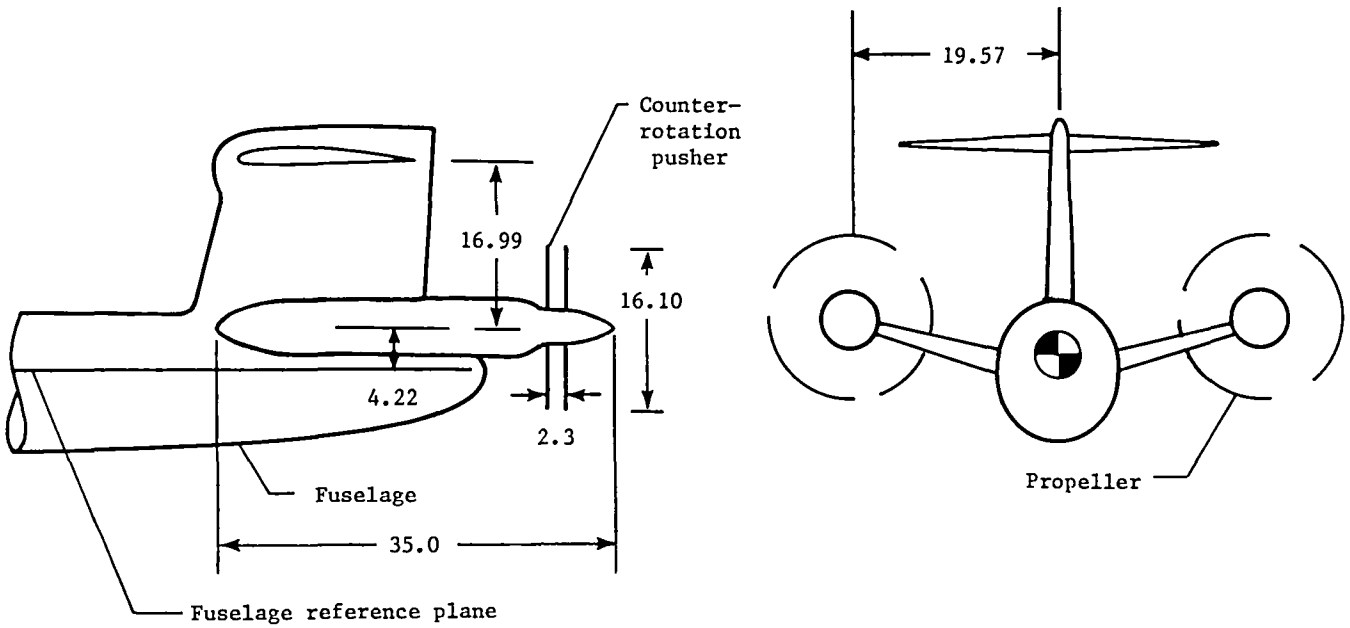

Figure 18.- Mounting arrangement and geometric characteristics of model-mounted pusher configuration. Dimensions are given in inches.

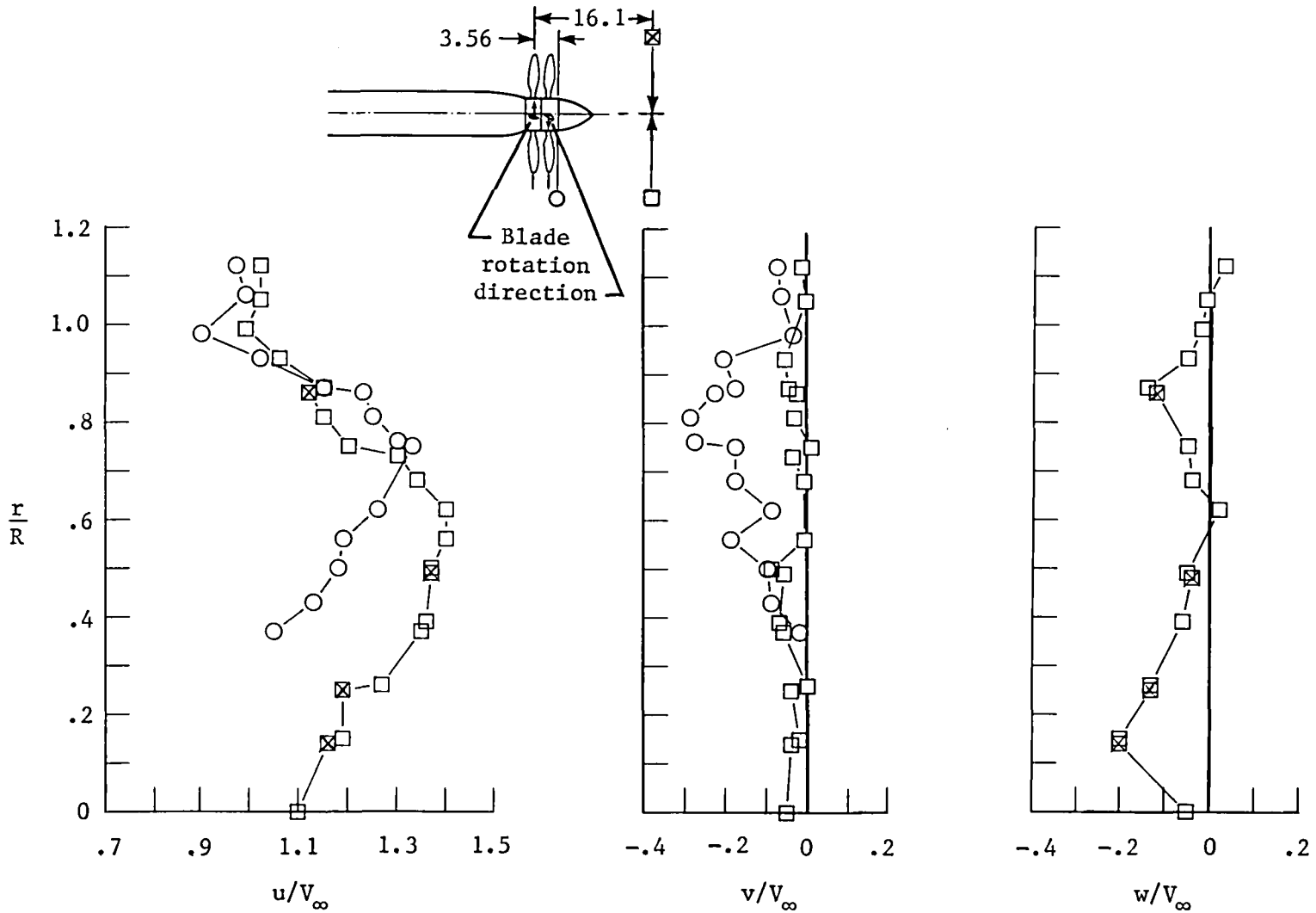

Figure 19.- Propeller flow-field velocity ratios near model-mounted counter-rotation pusher configuration. $\beta_{.75}$ = 41.34°/41.34°; J = 1.21; C_T = 0.56. Dimensions are given in inches.

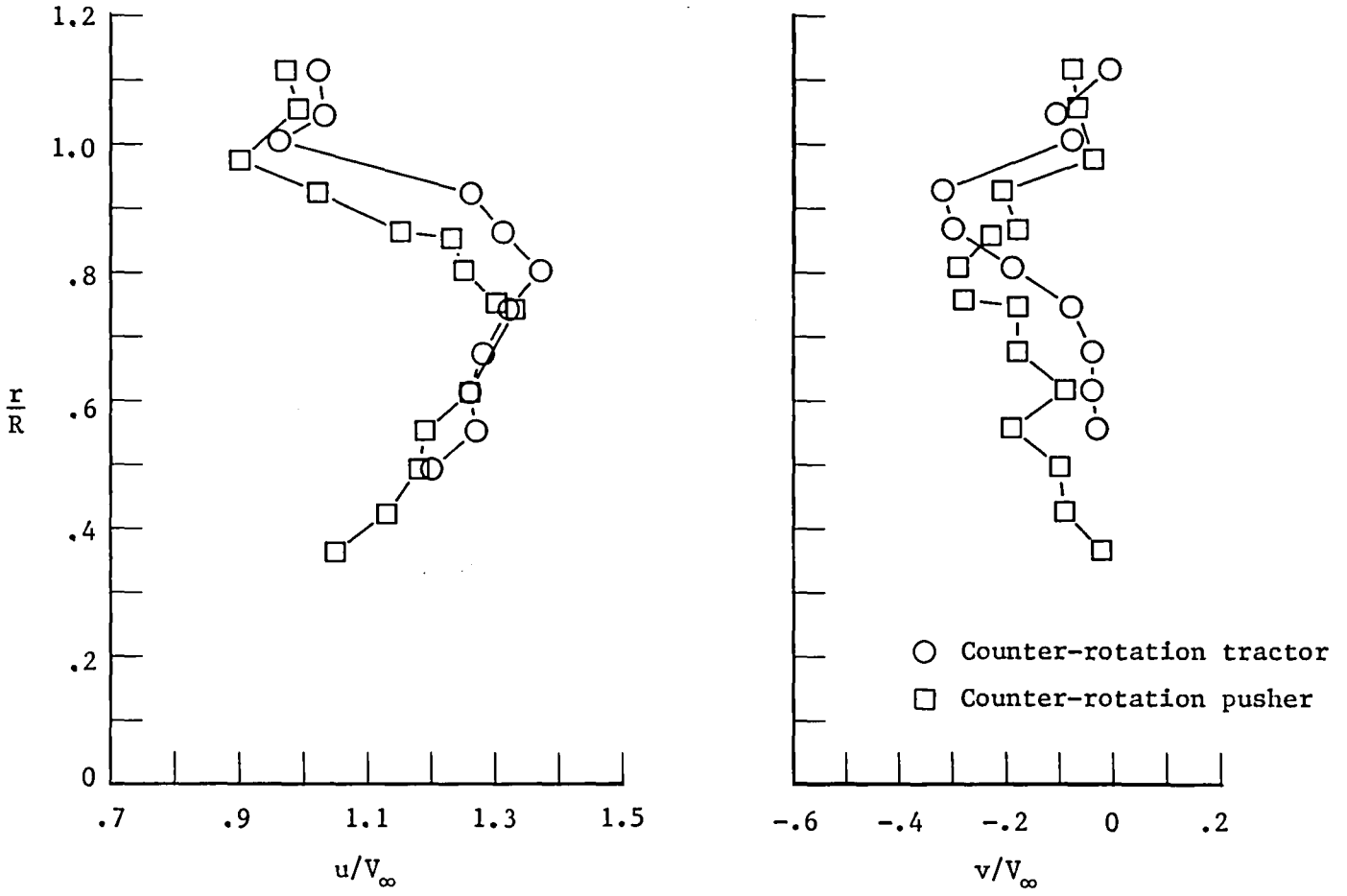

Figure 20.- Comparison of propeller flow fields 1.25 in. behind rear-propeller pitch change axis of counter-rotation tractor propeller/nacelle and model-mounted counter-rotation pusher configurations. $\beta_{.75}$ = 41.34°/41.34°; J = 1.21; C_T = 0.56.

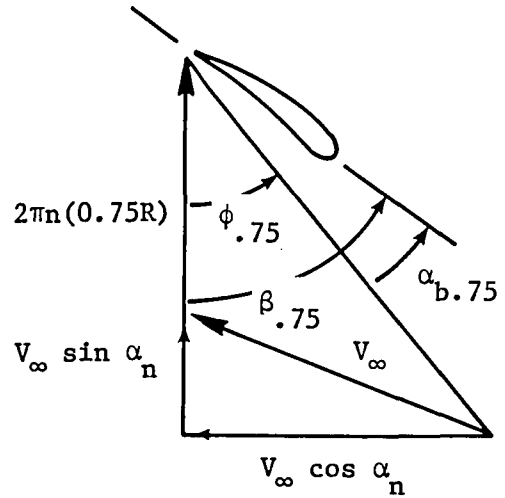

Downgoing blade

$$\alpha_{b.75} = \beta_{.75} - \phi_{.75}$$

$$2\pi n(0.75R) = \frac{0.75\pi V_\infty}{J}$$

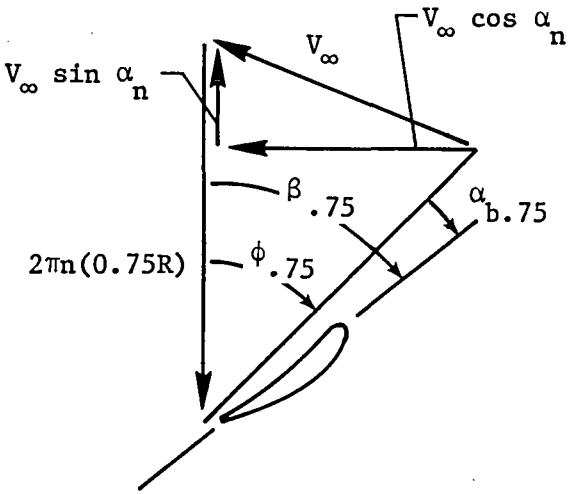

Upgoing blade

$$\phi_{.75} = \tan^{-1}\left(\frac{V_\infty \cos \alpha_n}{2\pi n(0.75R) + V_\infty \sin \alpha_n}\right)$$

$$\phi_{.75} = \tan^{-1}\left(\frac{V_\infty \cos \alpha_n}{2\pi n(0.75R) - V_\infty \sin \alpha_n}\right)$$

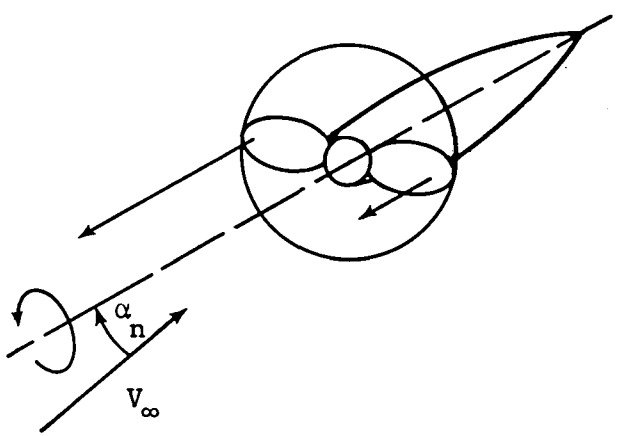

Figure 21.- Sketch illustrating origin of asymmetric thrust loads on propeller at angle of attack.

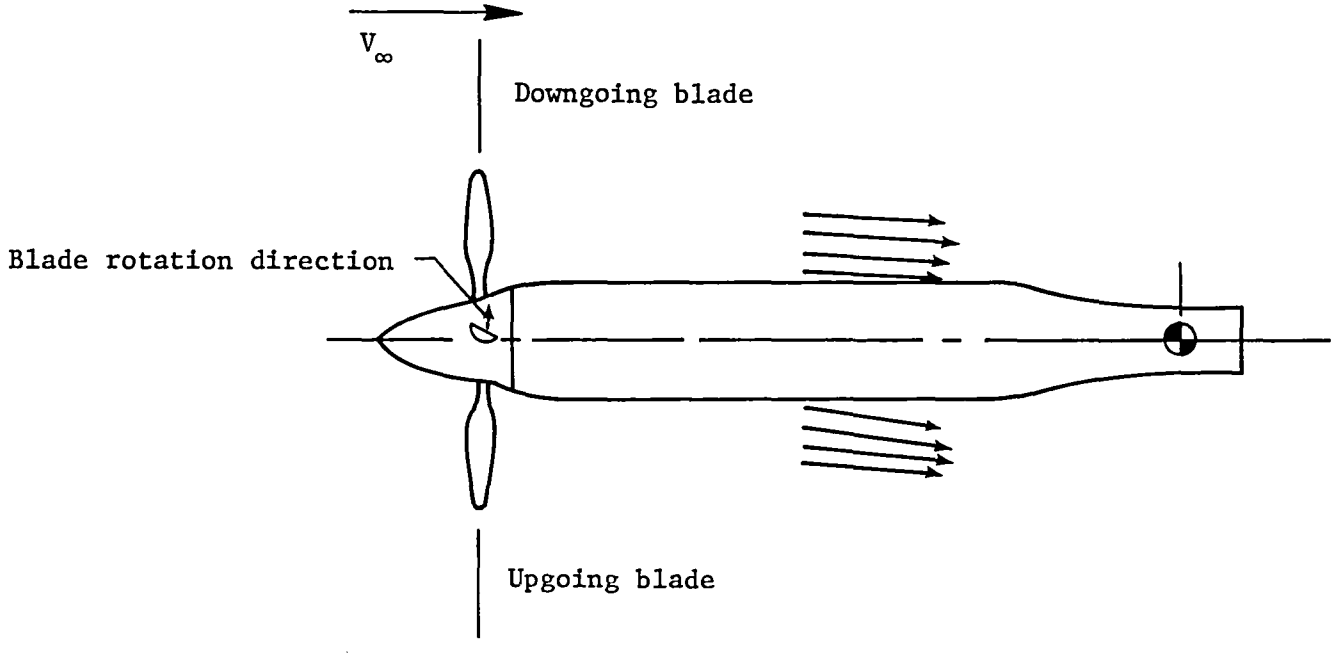

Figure 22.- Effect of nacelle angle of attack on propeller flow field, as viewed from above. $\beta_{.75} = 40.30°$; $J = 1.18$; $\alpha_n = 8°$.

○ 8-blade single-rotation propeller ($\beta_{.75}$ = 40.30°)

□ 4 × 4 blade counter-rotation propeller ($\beta_{.75}$ = 41.34°/41.34°)

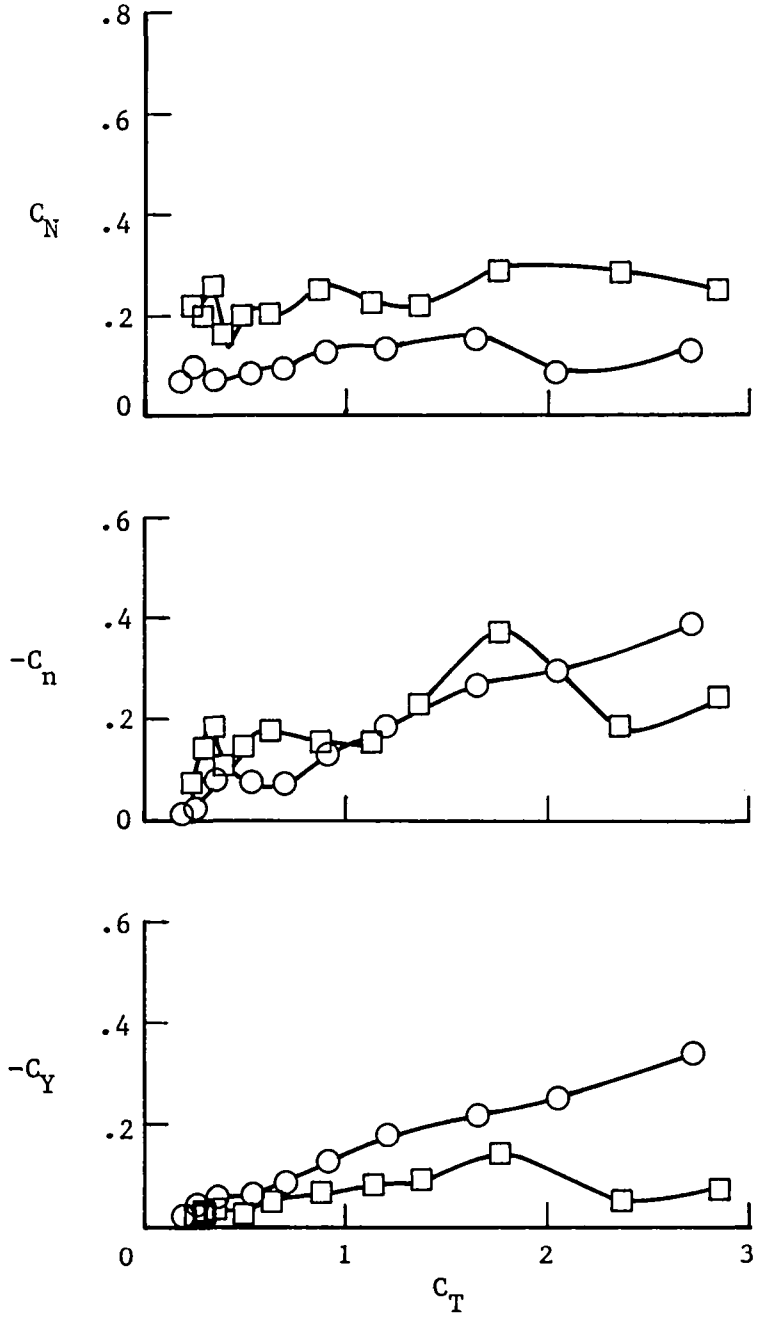

Figure 23.- Propeller characteristics at a nacelle angle of attack α_n of 10°.

1. Report No.	2. Government Accession No.	3. Recipient's Catalog No.
NASA TM-87656		

4. Title and Subtitle	5. Report Date
Low-Speed Wind-Tunnel Tests of Single- and Counter-Rotation Propellers	April 1986
	6. Performing Organization Code: 505-45-43-02
7. Author(s): Dana Morris Dunham, Garl L. Gentry, Jr., and Paul L. Coe, Jr.	8. Performing Organization Report No.: L-16077
9. Performing Organization Name and Address: NASA Langley Research Center, Hampton, VA 23665-5225	10. Work Unit No.
	11. Contract or Grant No.
12. Sponsoring Agency Name and Address: National Aeronautics and Space Administration, Washington, DC 20546-0001	13. Type of Report and Period Covered: Technical Memorandum
	14. Sponsoring Agency Code

15. Supplementary Notes

16. Abstract

A low-speed (Mach 0 to 0.3) wind-tunnel investigation was conducted to determine the basic performance, force and moment characteristics, and flow-field velocities of single- and counter-rotation propellers. Compared with the eight-blade single-rotation propeller, a four- by four- (4 × 4) blade counter-rotation propeller with the same blade design produced substantially higher thrust coefficients for the same blade angles and advance ratios. The results further indicated that ingestion of the wake from a supporting pylon for a pusher configuration produced no significant change in the propeller thrust performance for either the single- or counter-rotation propellers. A two-component laser velocimeter (LV) system was used to make detailed measurements of the propeller flow fields. Results show increasing slipstream velocities with increasing blade angle and decreasing advance ratio. Flow-field measurements for the counter-rotation propeller show that the rear propeller turned the flow in the opposite direction from the front propeller and, therefore, could eliminate the swirl component of velocity, as would be expected.

17. Key Words (Suggested by Authors(s))

Turboprop
Laser velocimeter (LV)
Single-rotation propeller
Counter-rotation propeller

18. Distribution Statement

Unclassified - Unlimited

Subject Category 02

19. Security Classif.(of this report)	20. Security Classif.(of this page)	21. No. of Pages	22. Price
Unclassified	Unclassified	44	A03

For sale by the National Technical Information Service, Springfield, Virginia 22161

NASA-Langley, 1986

National Aeronautics and
Space Administration
Code NIT-4

Washington, D.C.
20546-0001